RNA viruses that exploit self-cleaving ribozymes for translation initiation

María José López-Galiano[1,9], Olga Rueda[1,9], Sotaro Chiba[2], Marco Forgia[3], Beatriz Navarro[4], Amelia Cervera[1], Artem Babaian[5,6], Francesco Di Serio[4], Massimo Turina[7,8], Marcos de la Peña[1*]

[1] Instituto de Biología Molecular y Celular de Plantas, Universidad Politécnica de Valencia-CSIC, Valencia, Spain

[2] Graduate School of Bioagricultural Sciences, Nagoya University, Chikusa, Nagoya, Japan

[3] Institute for Sustainable Plant Protection, National Research Council of Italy, Torino, Italy

[4] Institute for Sustainable Plant Protection, National Research Council of Italy, Bari, Italy

[5] Department of Molecular Genetics, University of Toronto, Toronto, ON, Canada

[6] Terrence Donnelly Centre for Cellular & Biomolecular Research, University of Toronto, Toronto, ON, Canada

[7] Institute for Sustainable Plant Protection, National Research Council of Italy, Brescia, Italy

[8] Department of Plant Protection, School of Agriculture, The University of Jordan, Amman, Jordan

[9] These authors contributed equally

*corresponding author: rivero@ibmcp.upv.es

Abstract

Small self-cleaving ribozymes are catalytic RNAs originally discovered in viroid-like agents, which are replicating circular RNAs (circRNAs) postulated as relics of a prebiotic RNA world. In the last decade, however, small ribozymes have also been detected across the tree of life, from bacterial to human genomes, and more recently, in unusual circRNA viruses. Here we report the conserved occurrence of diverse small ribozymes within the linear genomes of typical double- and single-stranded RNA virus families from fungi and plants. Type I hammerhead ribozyme motifs occur in the 5'-UTR regions of chrysovirids and fusarivirids, displaying self-cleaving activity *in vitro* and *in vivo*. Similar hammerhead, as well as hepatitis delta and twister ribozymes, are also found in diverse megabirna-, hypo-, fusagra-, toti- or tombus-like viruses among others. The ribozymes occur not only as isolated motifs within UTRs but also as tandem pairs that encompass small RNA segments (186-399 nt) resembling Zetavirus-like sequences. *In vivo* characterization of the 5'-UTR with a ribozyme from a chrysovirid revealed that the RNA-cleaving activity is essential for protein translation initiation in fungi. Analogous experiments in plants with diverse ribozyme motifs indicated that just the presence of a self-cleaving activity can induce cap-independent translation. We conclude that RNA self-cleaving activity, historically linked to the rolling circle replication of viroid-like circRNAs, appears to be co-opted by linear RNA viruses for translational roles.

Introduction

RNA's dual nature as carrier of genetic information and biochemical catalyst has established it as a candidate molecule for the origin of life. RNA predates DNA, proteins and the genetic code in the primordial "RNA world" hypothesis[1–3]. Genetic remnants of this hypothetical RNA world would be the extant catalytic RNAs, such as the ribosomal RNAs, the RNAse P, or the small self-cleaving ribozymes. Therefore, the simplest RNA-based entities, such as viruses, viroids and other minimal mobile RNA genetic elements, are hypothesized to be living fossils of Earth's first life[4,5]. The simplest known ribozymes belong to the family of small (50-200 nt) self-cleaving RNAs, with nine well characterized members: the hammerhead (hhrbz)[6,7], hairpin (hprbz)[8], human Hepatitis Delta (dvrbz)[9], Varkud-Satellite (vsrbz)[10], glmS[11], twister (twrbz)[12], twister sister, hatchet and pistol[13] ribozymes. During the '80s, the first small ribozymes were described in infectious circRNAs of plants (hhrbz and hprbz in viroid-like agents), animals (dvrbz in Hepatitis Delta Virus) and fungi (vsrbz in a *Neurospora crassa* plasmid), but are also encoded in some DNA genomes[14,15]. In the last decade, these motifs have been discovered to be widespread in the DNA genomes of phages, bacteria, or eukaryotes[16–18], including the human genome[19,20]. The precise biological functions of many of these genomic ribozymes are not well understood, but numerous hhrbz, dvrbz and twrbz motifs strongly associate with autonomous and non-autonomous retrotransposons across plant and metazoan genomes[21–26].

Likely due to its simplicity[27], the hhrbz is one of the most frequent ribozymes detected in nucleic acids. It is composed of three double helixes (I to III) that surround a core of 15 conserved nucleotides, and folds into a γ-shaped helical junction where the loops of helix I and II interact[28,29]. Depending on the open-ended helix, three main circularly permuted topologies (type I, II, or III) are possible for the hhrbz (Fig. 1A), although examples of novel permuted forms have also been recently reported for this ribozyme[30,31]. The dvrbz, another small ribozyme widespread among DNA genomes, shows a characteristic nested double pseudoknot structure with five helical regions (Fig. 1B).

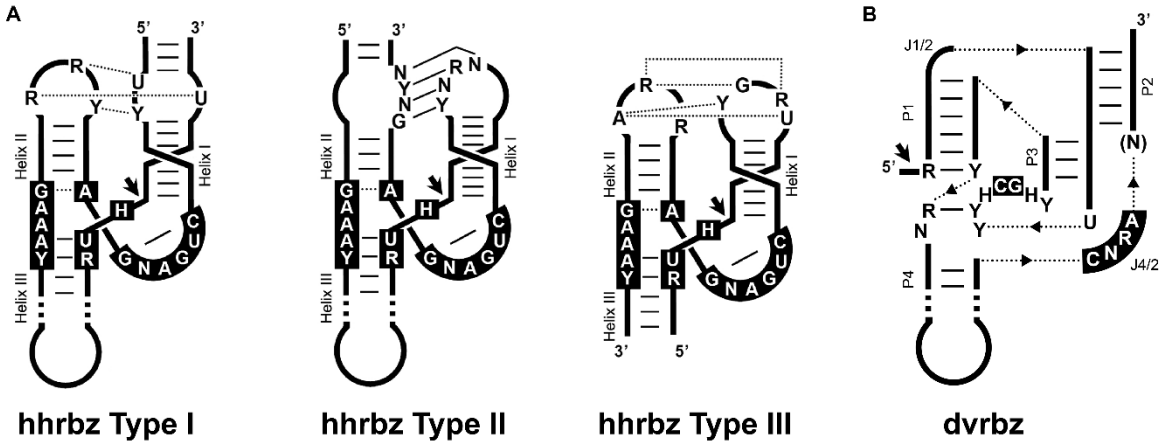

Fig. 1. Schematic representation of (A) the three hammerhead topologies (hhrbz Type I, II, and III) and (B) the hepatitis delta virus (dvrbz) ribozymes. The conserved nucleotides are shown in black boxes. Typical tertiary loop-loop interactions of the hhrbz are indicated (dotted and continuous lines refer to non-canonical and Watson–Crick base pairs, respectively). Dotted lines with triangles represent connections between the helixes. Helical stems and single-stranded junction strands are indicated. Black arrows indicate the self-cleavage site.

Sequencing and computing have driven an exponential growth in the characterized biodiversity of microbial life forms. This expansion has relied on the use of protein hallmark genes or ribosomal RNA. However, we are starting to appreciate the existence of an extant and highly diverse RNA world of minimal agents. Previous analyses have unveiled hundreds of novel circRNA genomes with self-cleaving ribozymes in either one or both polarities[32,33]. More recently, these minimal circRNA agents were expanded to thousands of viroid-like taxonomic units, including examples of novel RNA virus-viroid hybrids in fungi[31,34] or viroid-like obelisks in bacteria[35]. These discoveries blur the distinction between viroidal agents, ribozyme-bearing satellite viruses, and RNA viruses, but confirms the existence of a "modern RNA world" of mobile genetic elements of circRNA with and without small self-cleaving ribozymes[31].

Here, we extend the conserved occurrence of small self-cleaving ribozymes, notably specific variants of the type I hhrbz, to diverse families of viruses with linear RNA genomes from fungi and plants. These catalytic motifs do not appear to be involved in the classical role of RNA processing of intermediates during rolling-circle replication, but instead have been functionally co-opted to perform novel translational roles in the life cycle of linear RNA viruses.

Results

Type I hammerhead ribozymes in dsRNA viruses

In silico screening for the nine known families of small ribozyme structures in viral sequences deposited in public databases revealed conserved motifs across evolutionarily diverse RNA viruses (see Methods for full details). Notably, putative ribozyme motifs were identified in the *Chrysoviridae* family of multipartite dsRNA viruses, where 42% (96 out of 226 contigs >2 kb) of the alphachrysovirus sequences contain a distinct variant of the type I hhrbz class (Fig. 1). These motifs are usually located in the 5'-UTRs (positive strand) of each of the four RNA segments comprising the viral genome (Fig. 2A and Supplementary Table 1). Exceptionally, a few alphachrysoviral segments exhibit a second hhrbz at the 3'-UTR region of the RNA (ie. Raphanus sativus chrysovirus 1, RNA segments 1 and 3. Supplementary Table 1). However, no examples of small ribozymes were detected in any of the betachrysovirus sequences analyzed (134 contigs >2 kb).

Most type I hhrbzs have been previously reported in diverse eukaryotic retroelements[14,15,22,25,36], where they usually show a short helix III that prevents efficient self-cleavage of monomeric but not of dimeric hhrbz molecules[6,37]. However, chrysoviral type I hhrbzs show a longer helix III, resembling type I hhrbzs encoded in the DNA genomes of some bacteria/phages[16], fungi[22] and mammals[19]. The newly uncovered hhrbzs from chrysoviruses can be categorized into two conserved architectures with distinct properties (Fig. 2B); one third of the hhrbzs have long and stable helix II of 6 bp capped by a tetraloop and usually harboring a bulged adenosine in the middle of the stem, whereas two thirds show a short (1-2 bp stem) or even non-existent helix II (Fig. 2B and Supplementary Fig. 1).

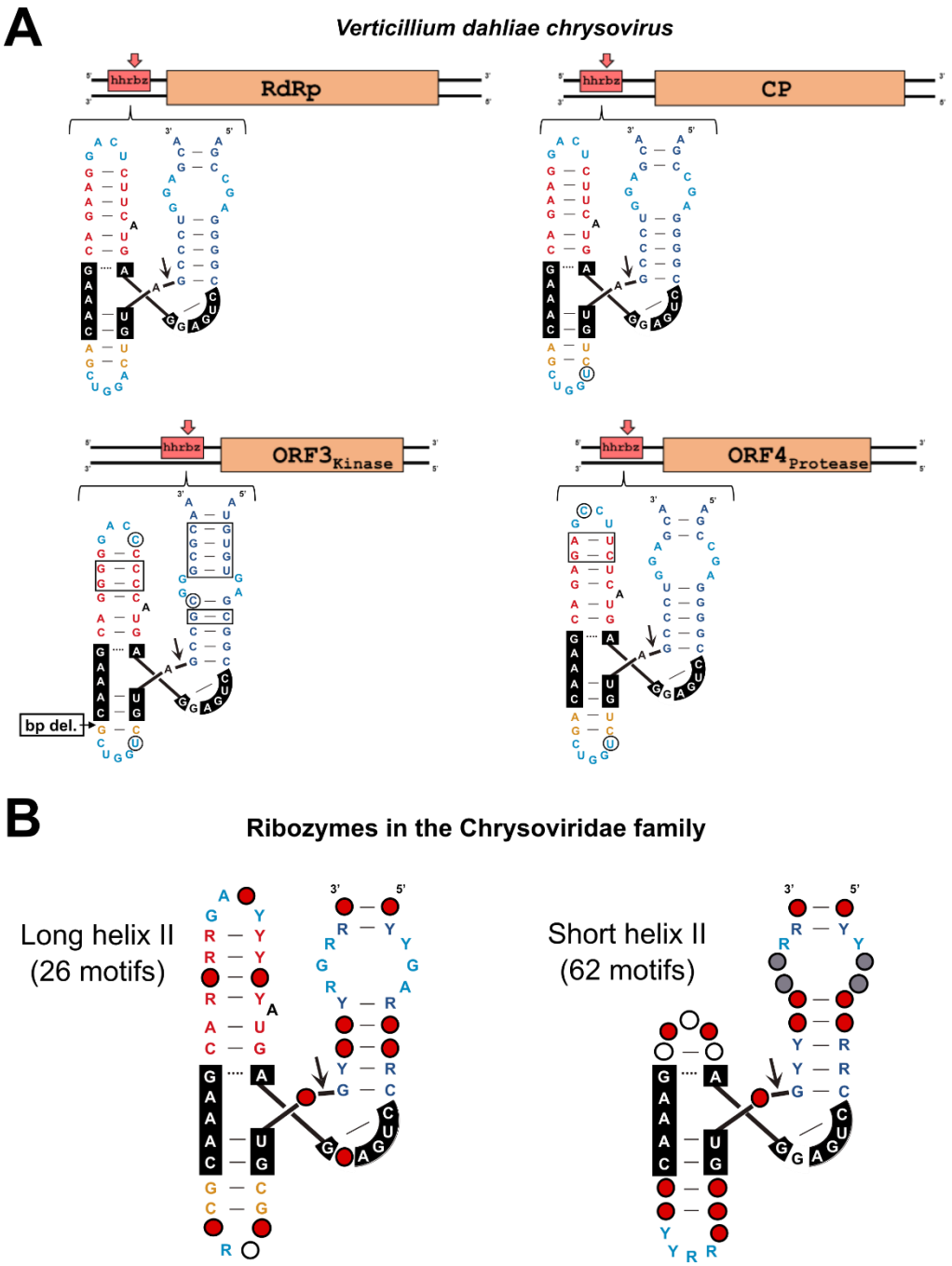

Fig. 2. Fungal and plant chrysovirus hammerhead ribozymes (hhrbz). (A) The multipartite Verticillium dahliae chrysovirus[38]contains type I hhrbzs in the 5'-UTRs of the 4 RNA segments that make up the viral genome. Nucleotide changes in the ribozyme motifs with respect to the hhrbz at the RNA 1 encoding the RNA-dependent RNA polymerase (RdRp) are indicated by circles (single changes) and rectangles (base-pair covariations) (B) A summary of the covariance models for the two hhrbz architectures detected among most chrysoviruses. Red, grey and white dots refer to nucleotides present in more than 97%, 75% or 50% of the sequences, respectively. Y: C or U. R: G or A (See Supplementary Fig. 1A for details). CP, coat protein. ORF, open reading frame.

In vitro analyses confirmed that chrysovirus hhrbzs with long helix II self-cleave efficiently during transcription (k_{obs}~2-3 min^{-1}) (Fig. 3A). However, the observed rates of self-cleavage for the hhrbz with short (1 bp) or absent helix II were either low (k_{obs} ~10^{-2} min^{-1}) or very low (k_{obs} ~10^{-3} min^{-1}), respectively (Fig. 3B, C). These minimal rates of cleavage were observed during co-transcriptional experiments, but similar results were observed under post-transcriptional conditions, even at high pH (8.5) and Mg^{+2} concentrations (10 mM) (Supplementary Fig. 2).

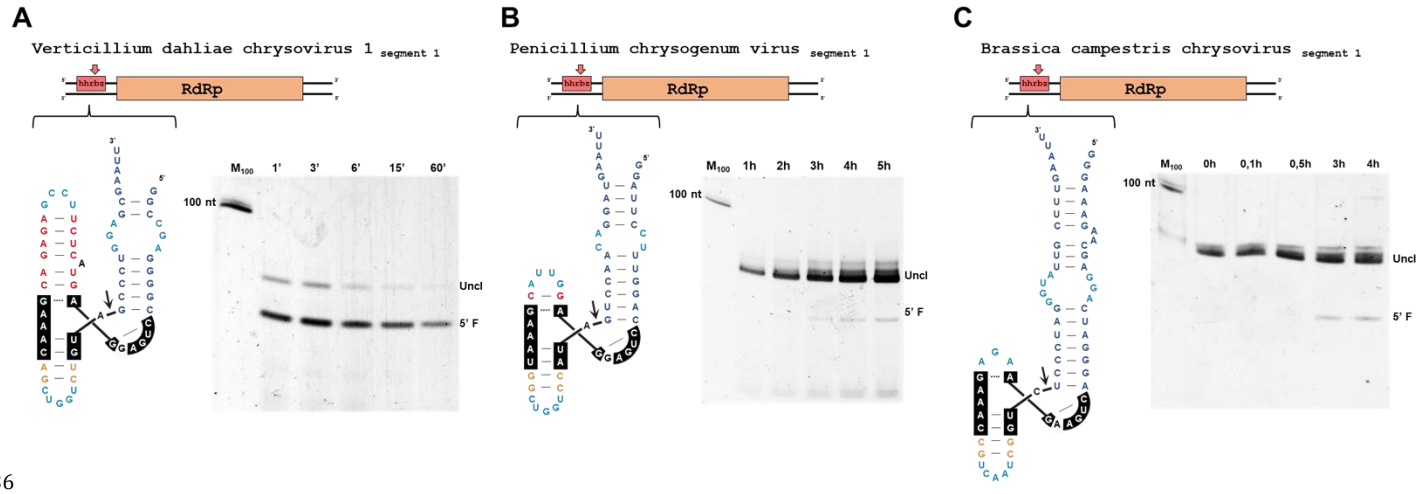

Fig. 3. Self-cleavage kinetics of hammerhead ribozymes from fungal and plant chrysoviruses. (A) long helix II, (B) short helix II, or (C) totally absent helix II hammerhead ribozymes are catalytically competent *in vitro* but show distinct self-cleaving efficiencies. RdRp, RNA-dependent RNA polymerase. (A) and (B) correspond to co-transcriptional cleavage analysis under standard conditions (pH 7.5, 1 mM Mg^{2+}), whereas (C) shows a post-transcriptional assay performed at higher pH (8.5) and Mg^{2+} concentration (10 mM) to increase its self-cleaving capability.

Other ds and ssRNA viruses encode hammerhead, but also deltavirus and twister ribozyme motifs

Fusariviruses are a family of mycoviruses with monopartite ssRNA genomes that encode one to four ORFs[39,40]. Our bioinformatic analyses found that 114 of the 156 analyzed fusariviral sequences encode one or more type I hhrbzs, totaling 160 identified motifs (Supplementary Table 1). These hhrbz sequences and their helix sizes exhibit significant variability across viral genomes. As observed for chrysoviruses, they either follow a canonical type I hhrbz architecture, with medium size helixes I, II and

152 III (4-8 bp stems), or variants with short helix II (1-2 bp stems) (Supplementary Fig.
153 1B, C). These observations suggest high and low self-cleavage efficiency, respectively,
154 for each of the two architectures. Again, fusariviral ribozymes occur in the untranslated
155 regions preceding most viral ORFs (Fig. 4A and Supplementary Fig. 3A). We made
156 similar observations in the family of bipartite dsRNA megabirnaviruses[41], which show
157 the presence of slightly different variants of the type I hhrbz with longer helix II
158 (Supplementary Fig. 2D, 3B). The motifs occur again in the large 5'-UTR of diverse
159 megabirnavirus RNA segments (17 out of 32 analyzed contigs) (Supplementary Table
160 1). Interestingly, not only hhrbz motifs, but also an example of a *bonafide* dvrbz was
161 detected in a genomic segment of the Rhizoctonia cerealis megabirnavirus-like RNA
162 (Fig. 4B, Supplementary Fig. 2B). Similarly, instances of dvrbz, type I hhrbz and even
163 twrbz motifs, were detected in the dsRNA genomes of diverse totiviruses. In these
164 examples, however, the motifs were usually found as pairs of ribozymes (either from
165 the same or different classes) arranged in close tandem separated by 186-399 nt (Fig.
166 4C). This arrangement echoes that observed in plant and animal retrozymes, where
167 closely spaced tandem ribozyme pairs encoded in DNA genomes produce small
168 circRNAs[24,25]. In the case of these totiviruses, the predicted circRNAs (i) can adopt
169 stable rod-like structures, (ii) have nucleotide sizes that are multiples of three, and (iii)
170 contain ORFs without stop codons, potentially encoding a never-ending polypeptide in
171 the positive strand (Fig. 4C, Supplementary Fig. 4). These three features somewhat
172 resemble those described for the intriguing group of viroid-like Zetaviruses genomes
173 detected in diverse environmental metatranscriptomic studies[31,32] (Supplementary
174 Fig. 4D). However, predicted circRNAs in totivirus-like genomes usually lack a key
175 characteristic of Zetaviruses, as they do not retain any of the flanking ribozymes within
176 their circular sequences[31,34].

177 Our bioinformatic analyses also revealed the presence of analogous type I hhrbzs in
178 the UTRs of some dsRNA genomes from additional fungal viral families, such as
179 fusagraviruses and hypoviruses (Supplementary Table 1). Moreover, we also detected
180 diverse variants of the twister ribozyme at the 5'-UTRs of some phlegi- (ie. Rhizoctonia
181 zeae dsRNA virus 1 and 2)[42] or tombus-like viruses from diverse soil and plant-

associated microbial communities (Supplementary Fig. 5). Altogether, these results confirm the prevalence of small self-cleaving ribozymes encoded within the linear RNA genomes of diverse fungal and plant viruses.

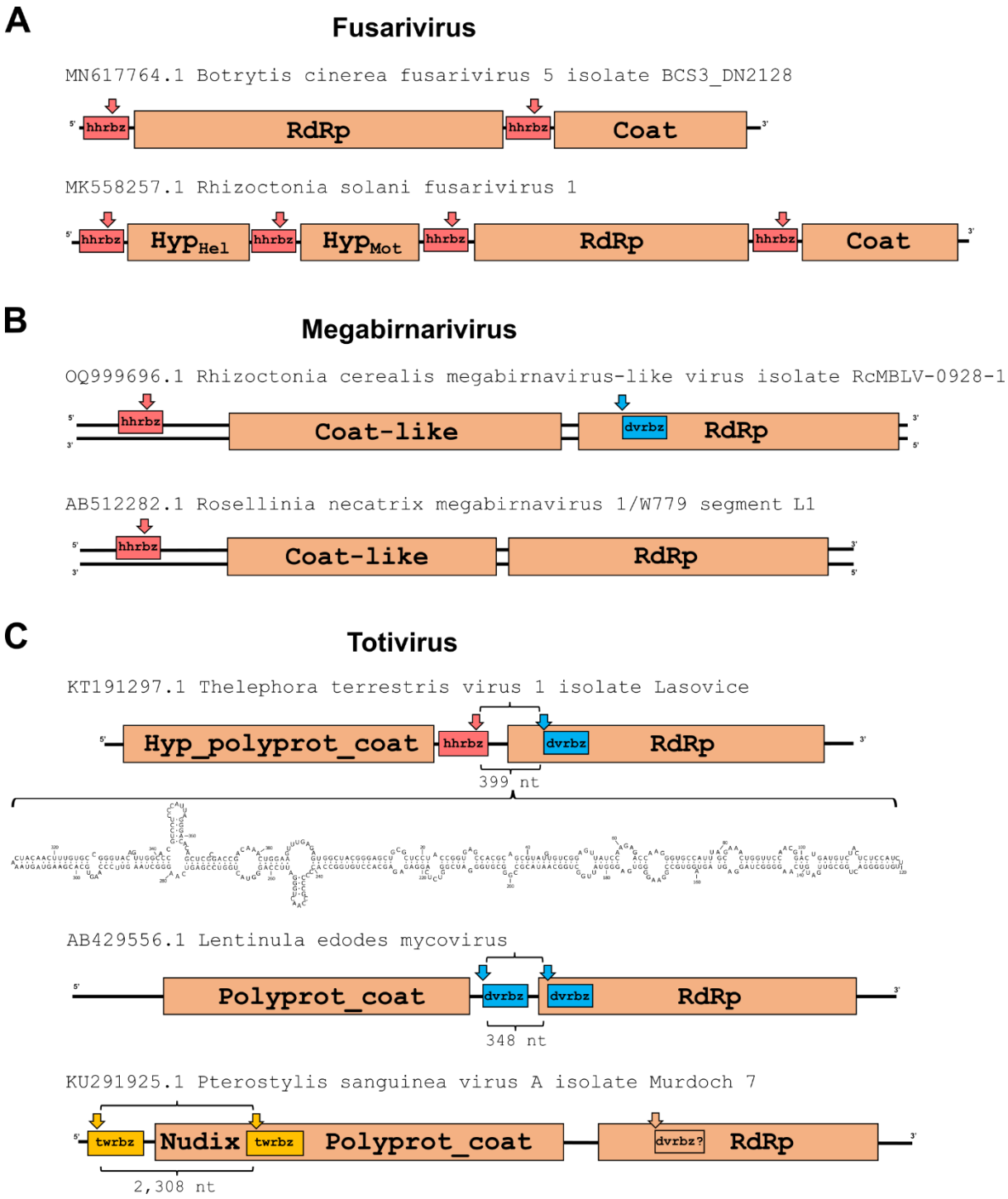

Fig. 4. Small ribozymes are widespread in fungal ss and dsRNA viruses with linear genomes. (A) fusariviruses, (B) megabirnaviruses and (C) totiviruses encode conserved self-cleaving ribozymes of the

188 hhrbz, dvrbz and twrbz classes. In totivirus genomes, pairs of hammerhead and delta self-cleaving
189 ribozymes occur close to each other (~189-399 nt). Similar arrangements of close ribozymes in tandem
190 responsible of circRNA formation have been previously identified in plant[24] and metazoan[25] genomes,
191 suggesting that totivirus ribozymes would allow the generation of small circRNAs, as depicted for
192 Telephora terrestris virus 1 (See Supplementary Fig. 4 for more details).

193

194 Hammerhead ribozymes in RNA viruses show self-cleaving activity *in vivo*

195 Given the widespread occurrence of type I hhrbzs among chrysovirids and fusarivirids,
196 we chose to look for *in vivo* evidence of ribozyme self-cleaving activity during viral
197 infection. We selected two chrysoviruses (either infecting a plant or a fungus) and one
198 fungal fusarivirus as examples of ds and ssRNA viruses with hhrbzs in different 5'-UTRs
199 regions, respectively.

200 Brassica campestris chrysovirus 1 (BcCV1) is a tripartite dsRNA chrysovirus infecting
201 brassica plants[43], which shows conserved hhrbzs (short helix II variants with a minimal
202 self-cleaving activity *in vitro*, see above) in the 5'-UTRs of each RNA segment. The
203 expected cleavage sites of the hhrbzs map at positions 58, 60 and 60 of RNA segments
204 1, 2 and 3, respectively (Supplementary Fig. 6A). Rapid amplification of cDNA ends
205 (RACE) experiments using total RNA from a BcCV1-infected *B. oleracea* plant generated
206 two amplification products for each of the chrysovirus RNAs, which are more evident
207 in the case of RNA2 and RNA3 (Supplementary Fig. 6B). Cloning and sequencing of the
208 amplicons confirmed the existence, for each genomic RNA segment, of molecules with
209 two different 5' ends, one corresponding to the expected viral full-length RNA segment,
210 and the other one with the self-cleavage site predicted for the respective embedded
211 ribozyme (Supplementary Fig. 6C).

212 The recently characterized Gnomognopsis castanea chrysovirus 1 (GcCV1) has 4
213 genomic segments encoding one ORF each, except for the bicistronic RNA3[44]. We
214 detected the presence of 5 different hhrbz motifs (long helix II variants with efficient
215 self-cleaving activity *in vitro*, see above), one in each 5'-UTR preceding an ORF
216 (Supplementary Fig. 7). Here, RACE experiments carried out on total RNA extracted
217 from an infected fungus isolate showed that the population of viral RNAs is also
218 composed of RNA segments with two different 5' termini, as supported by clones either

219 mapping to the expected 5' end of the genomic RNA, or to the predicted 5' site of self-
220 cleavage of each hhrbz (Supplementary Fig. 7). Such a mix of RNA molecules with two
221 different ends is particularly evident for RNA2, which gives two abundant and distinct
222 bands in PCR RACE amplifications (Supplementary Fig. 7E). It is of note that, in this
223 virus, the two copies of hhrbz present in each one of the two UTRs of the bicistronic
224 RNA3 were found to self-cleave *in vivo* at their predicted sites.

225 Finally, Pleospora tiphycola fusarivirus 1 (PtFV1) is a ssRNA virus present in an
226 ascomycetes fungus isolated from the seagrass *Posidonia oceanica*[45]. Members of the
227 recently established *Fusariviridae* family are a group of non-segmented viruses with
228 heterogeneous genome organization according to the genus they belong to[40]. The RNA
229 genome of PtFV1 can potentially express up to three proteins from three distinct
230 ORFs[45]. It also contains a predicted type I hhrbz with a short helix II, similar to the
231 Penicilium chrysogenum virus ribozyme (Fig. 3B). The catalytic RNA essentially spans
232 the entire small intergenic UTR (66 nt), with the self-cleavage site (position 4,735) just
233 7 nucleotides upstream of the proposed ORF2 start codon (position 4,742). RACE
234 analysis using reverse transcription products primed around 200 nt downstream the
235 cutting site confirmed the existence *in vivo* of an RNA species with the predicted 5' end
236 after self-cleavage (Supplementary Fig. 8A). Moreover, northern blot analysis showed
237 the accumulation of a positive-sense RNA fragment of a size compatible with that of a
238 subgenomic RNA originated by self-cleavage of the ribozyme (Supplementary Fig. 8B).
239 Overall, experiments with total RNA purified from either infected plants or fungi
240 followed by RACE analyses confirm that the population of viral RNA genomes *in vivo* is
241 heterogeneous, being composed of uncleaved and self-cleaved RNA molecules.

242

243 Hammerhead ribozyme self-cleavage in a chrysovirus UTR allows cap-
244 independent translation

245 Translation initiation activity, presumably via some kind of internal ribosome entry
246 site (IRES) element, has been proposed for the 5'-UTR and subsequent 72 nt of coding

247 region of fungal dsRNA viruses such as chrysoviruses and hypoviruses[46]. Among these,
248 the 5'-UTR of the alphachrysovirus Helminthosporium victoriae virus 145S (HvV145S)
249 RNA2 was suggested to carry an IRES-like element. We found that, as in most
250 alphachrysoviruses, the 5'-UTRs of the HvV145S RNA segments also contain conserved
251 type I hhrbzs (Supplementary Table 1, Fig. 5A). These ribozymes correspond to the
252 hhrbz variants with long helix II (Fig. 2B), which are expected to reach efficient self-
253 cleaving activity *in vitro* and *in vivo*. To understand whether hhrbzs are directly
254 involved in protein translation initiation, on- and off-target mutations were introduced
255 into the self-cleaving motif and analyzed *in vivo*. The transgenic expression of
256 bicistronic RNAs in *Cryphonectria parasitica* mycelia was carried out as previously
257 described[46], in which the upstream ORluc and downstream OFluc genes were
258 translated in a cap-dependent and cap-independent manner, respectively (Fig. 5B).
259 The original HvV145S-2 5'-UTR sequence and its truncated variants in the 5' proximal
260 region preceding the ribozyme (Δ60 and Δ120) showed similar ratios of OFluc to ORluc
261 chemiluminescence intensity (RLU), suggesting that this off-target 5' region is
262 dispensable for translation initiation (Fig. 5D). In contrast, the deletion of the whole
263 region corresponding to the hhrbz motif (Δ124-183) abolished translation initiation of
264 OFluc, resulting in a significantly lower OFluc/ORluc RLU ratio. In addition, either a
265 single point mutation in the UTR ribozyme at position G159, the general base catalyst
266 in the self-cleavage reaction[29], or deletion of 5 essential nucleotides, including the
267 conserved U-turn motif[47] of the catalytic core of the ribozyme (Δ134-138), supressed
268 the translation initiation ability observed for the wt 5'-UTR sequence carrying the
269 catalytically competent hhrbz (Fig. 5C and D).

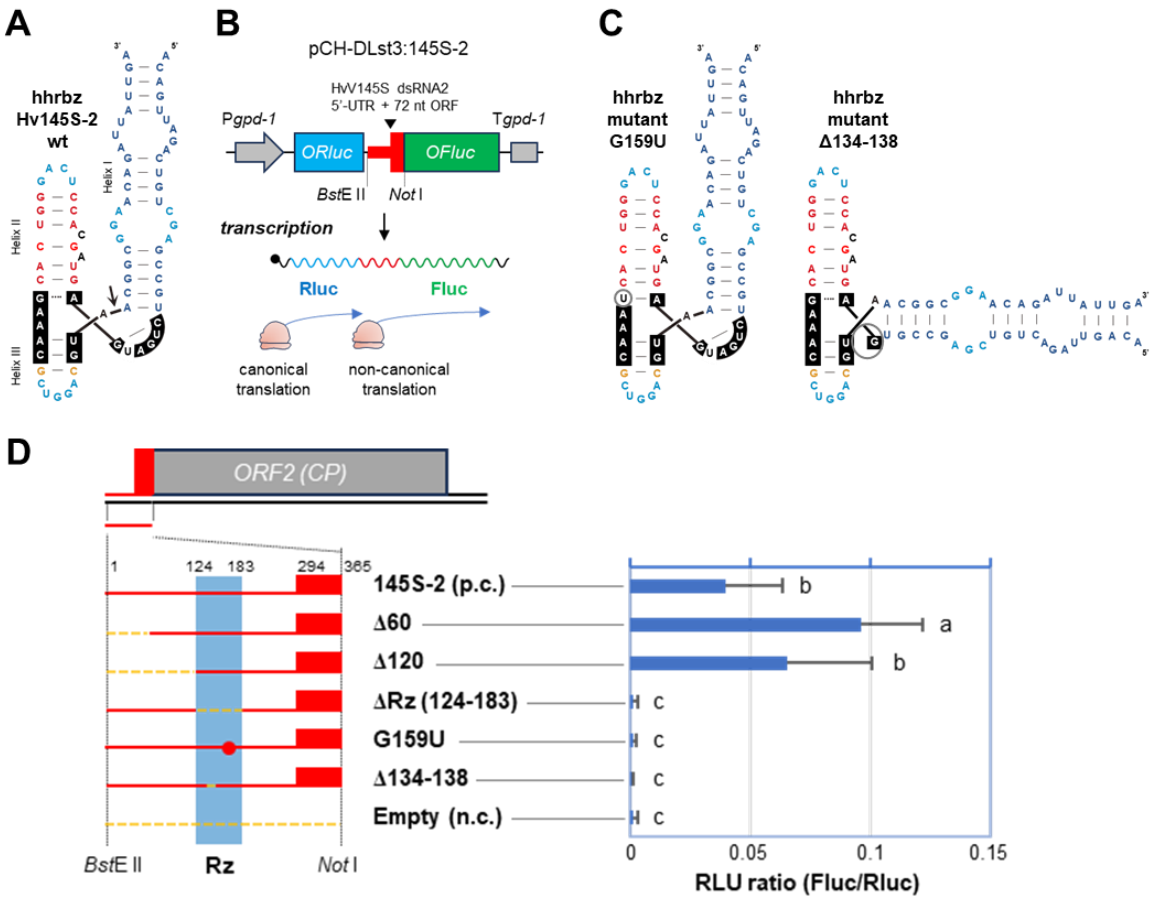

Fig. 5. Mutational analyses of the hammerhead ribozyme present in the 5'-UTR of the chrysovirus HvV145S RNA2. (A) Predicted structure of the HvV145S hammerhead ribozyme (hhrbz) present in the 5'-UTR of the RNA2. (B) A bicistronic dual-luciferase reporter system in fungal mycelia for investigation of the cap-independent initiation activity located at the 5'-UTR and coding region (72 nt) of HvV145S dsRNA2. Codon-optimized Renilla luciferase (ORluc, blue box) and firefly luciferase (OFluc, green box) genes are translated either in a canonical (cap-dependent) or a non-canonical (cap-independent) manner, respectively. Red line and box indicate HvV145S-2 sequence. (C) Predicted secondary structures of the 145S-2 hhrbz mutants containing either a substitution (left, G159U) or a deletion (right, Δ134-138), as indicated with grey circles. (D) Left, schematic representation of the 5'-UTR and first 72 nt of coding region (in red) of HvV145S-2 (in grey) used for the bicistronic dual-luciferase reporter system. The details of the mutations are represented at the bottom as the sequence variant names. Right,

282 dual luciferase reporter assay results for each construct showing the ratio of luminescent intensities
283 (Fluc RLU/Rluc RLU). p.c., positive control, n.c., negative control.

284

285 Diverse small self-cleaving RNA motifs induce translation initiation in plant
286 cells

287 To further investigate whether the observed effect of the chrysoviral hhrbz on protein
288 translation is specifically due the RNA self-cleaving activity or any other domains
289 present within the viral UTR, we employed a similar dual-luciferase reporter system
290 designed for its expression in agroinfiltrated *N. benthamiana* plant cells[48]. The
291 bicistronic constructs contained the Rluc and Fluc genes under the control of 35S
292 promoter and separated by a small (~150 bp) non-coding spacer either containing a
293 standard Multiple Cloning Site sequence (85 bp) or different small self-cleaving motifs
294 (~85-110 bp), such as type I hhrbzs from a plant (BrcCV1) and a fungal (VdCV1)
295 chrysovirus, from a megabirnavirus (RnMBV1) or from a human gene intron (the HH9
296 motif[19]). In addition, a dvrbz from an animal deltavirus (NewtDV, genomic sequence)
297 was also assayed (Fig. 6A). As expected, the construct carrying the MCS sequence
298 chosen as a negative control showed no noticeable OFluc/ORluc ratio (Fig. 6B).
299 However, constructs with chrysoviral hhrbz motifs produced a weak but discernible
300 signal, while a much higher ratio was observed with the Rosellinia necatrix
301 megabirnavirus 1 (RnMBV1) hhrbz. Moreover, a construct carrying the dvrbz also
302 showed a significant signal of OFluc protein expression (~0.4%). In contrast, assays
303 using the HH9 ribozyme, a fast self-cleaving hhrbz[19], resulted in minimal Fluc/Rluc
304 ratios. However, it should be noted that both Fluc and Rluc raw signals for the construct
305 containing the HH9 ribozyme were consistently one order of magnitude lower than the
306 observed one for other constructs, suggesting that HH9 activity interferes with the
307 normal expression of the reporter system.

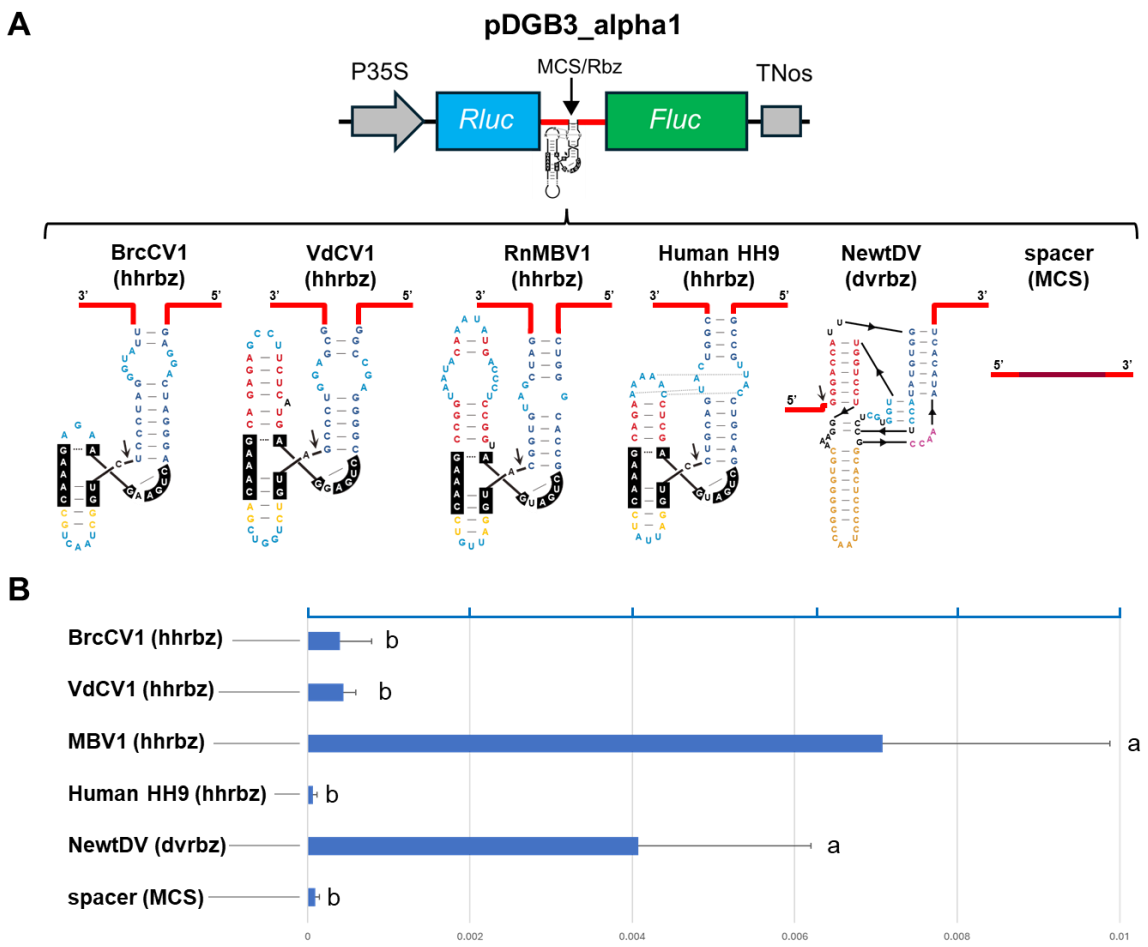

Fig. 6. Analysis of RNA self-cleavage on a dual-luciferase reporter expression in *N. benthamiana* leaves. (A) Schematic representation of the dual-luciferase reporter construct used in the study, with the Rluc and Fluc genes separated by a short DNA region (~130 bp) including either a MCS sequence (49 bp) or various self-cleaving RNA motifs, such as hammerhead ribozymes (hhrbz) from plant (BrcCV1) and fungal (VdCV1) chrysoviruses, a megabirnavirus (RnMBV1), a human gene intron (HH9), a deltavirus ribozyme (dvrbz) from NewtDV, and a negative control construct just containing MCS sequence. (B). dual luciferase reporter assay results for each construct agroinfiltrated in plants showing the ratio of luminescent intensities (Fluc RLU/Rluc RLU).

Discussion

Almost four decades after their discovery[6,7], the origins and evolutionary history of small self-cleaving ribozymes remain a complex puzzle. It is assumed that tiny RNAs

capable of sequence-specific cleavage and ligation could be among the first catalytic motifs to emerge during the RNA world, with a role in the replication of primordial RNA genomes[49]. Our knowledge about small ribozymes has been mostly limited to those from a unique family of a few viroid-like circRNAs (~15 species). In the last years, however, small catalytic RNAs have been found as ubiquitous motifs encoded in the DNA genomes of organisms throughout the tree of life[16,50] and, more recently, within thousands of novel viroid-like circRNAs in either eukaryotic or prokaryotic hosts[31–35]. Thus, this plethora of catalytic motifs are likely expected to have more biological roles beyond multimer self-processing.

In this work, we have expanded our knowledge about the occurrence of small ribozymes to typical ss- and dsRNA viruses with linear genomes. Notably, hundreds of novel variants of the type I hhrbz are found to be conserved in the 5'-UTRs of fungal and plant RNA viruses belonging to the *Chrysoviridae* and *Fusariviridae* families. It should be highlighted that nearly all hhrbz motifs previously detected in infectious circRNAs, such as plant viral satellites and viroids[51], obelisks[35], deltaviruses[52], ambiviruses or mitoviruses[31,34], correspond to the type III architecture, whereas type I hhrbzs are usually DNA-encoded motifs present in the genomes of either bacteria and bacteriophages[16,17,53] or metazoans[19,22,25,36]. On the other hand, natural hhrbzs adopt a similar three-way junction fold with conserved loop-loop interactions between helixes I and II (Fig. 1), which are crucial to achieve high activity under *in vivo* low magnesium concentrations [28,29,54]. The new viral type I hhrbzs described in this work, however, do not seem to have kept any of the typical loop-loop interactions conserved in known hhrbzs (Fig. 1) or in other three-helical RNAs with remote tertiary contacts[55]. Moreover, stem lengths of helix II in viral hhrbzs are either slightly longer (6-8 bp) or shorter (0-2 bp) than the ones present in most type I hhrbzs (4-5 bp) (Fig. 2B). These observations, together with a medium to low *in vitro* self-cleaving activity for viral hhrbzs, point to a lack of any clear loop-loop interactions in these motifs. These viral hhrbzs are however functional *in vivo*, as revealed by the co-existence of uncleaved and cleaved RNA genomes in plant and fungal infected cells, indicating that viral sub-

350 genomic RNAs arise through a novel mechanism catalyzed by small self-cleaving
351 ribozymes.

352 Regarding their biological role, most of the hhrbzs reported here are small motifs (50-
353 70 nt), which nevertheless can span a significant portion of the viral UTR sequences
354 (usually ~100-300 nt) where they are embedded. It has been proposed that, among
355 other functions, these 5'-UTR are involved in cap-independent translation initiation
356 acting as novel IRES-like elements[46]. Our deletion mutants of a chrysoviral UTR show
357 that the hhrbz motif (nucleotides 124-182) is specifically required for translation
358 initiation function. More intriguingly, a single point mutation in the catalytic G base
359 within the hhrbz core (known to inhibit RNA catalysis without altering the whole
360 ribozyme structure[56]) was enough to abolish the protein expression observed with the
361 wild-type UTR. This result suggests that self-cleaving activity would be crucial for the
362 role of the UTR in cap-independent translation. Consequently, we advance that viral
363 ribozymes may allow translation initiation thanks to their self-cleaving activity
364 through an unknown mechanism. As a second alternative, we can also envisage that a
365 mutation preventing self-cleavage may indeed affect, albeit minimally, the fold of the
366 hhrbz, which could disrupt a potential role as an IRES-like structure. To better
367 understand the role of RNA catalysis in eukaryotic translation initiation, we moved to
368 a similar bicistronic reporter system using plants instead of fungal protoplasts. This
369 new approach was based solely on the presence of isolated small ribozyme motifs
370 within dual-luciferase constructs and in the absence of any additional viral UTR
371 sequence. Interestingly, the presence of viral self-cleaving motifs alone was, in most
372 cases, sufficient to promote detectable translation initiation in plants when compared
373 with the construct lacking any ribozyme. These results, however, should be interpreted
374 with caution. First, the translation ratios of classic luciferase genes obtained in plants
375 with ribozyme-only constructs were modest (usually below 1%) relative to those
376 achieved with the full chrysoviral UTR (including 72-nt coding region) obtained with
377 codon optimized luciferase genes in fungi[46] (~4%-8%). Second, not all ribozymes
378 behaved equally, as translation levels were really low for the chrysovirus hhrbz
379 (~0.05%) but more evident for the megabirnavirus hhrbz or the newt dvrbz (0.4–

380 0.5%). Third, the hhrbz derived from the human genome (HH9) not only failed to
381 enhance Fluc expression but caused an overall reduction in luciferase activity from
382 both reporters, suggesting a detrimental effect on the whole mRNA stability and
383 expression. Altogether, these results indicate that the self-cleaving activity can
384 promote translation initiation, although the magnitude of this effect appears to depend
385 on the specific ribozyme context, biological system and self-cleaving efficiency. In this
386 regard, direct links between RNA self-cleaving motifs and eukaryotic protein
387 translation have been already advanced in the literature. Notably, the dvrbz present in
388 the 5' end of various eukaryotic retrotransposons has been reported to promote
389 protein translation initiation[21]. Consequently, this activity would mirror the
390 mechanism we describe here in RNA viruses.

391 The noticeable differences in protein expression found for different catalytic RNA
392 motifs suggest that self-cleaving activity could be a necessary condition but not
393 sufficient. These observations imply that the precise ribozyme sequence and/or
394 structure may jointly contribute to translation initiation. In this context, the global
395 architecture and topology of the type I hhrbz detected in RNA viruses shows clear
396 structural similarity with the core domains of diverse viral IRES elements, such as
397 those from picornaviruses[57], the encephalomyocarditis virus (EMCV)[58,59] or the
398 Hepatitis A virus (HAV)[60,61] (Supplementary Fig. 9), suggesting that not only the self-
399 cleaving activity but also the hhrbz ribozyme fold itself may have a potential role in the
400 recruitment of some translation initiation factors. This possibility could be extended to
401 the dvrbz, which despite clear structural differences with the hhrbz, they all share a
402 similar compact three-helical junction topology (where two helices coaxially stack and
403 the third helix runs parallel to the major axis of the Y-like structure) characteristic of
404 the core domain of diverse IRESs (Supplementary Fig. 10)[55].

405 Altogether, our data reveal a novel and unexpected activity in linear RNA viruses,
406 whereby the genomic RNA undergoes self-cleavage at one or more sites during the
407 viral life cycle. This cleavage sacrifices full genomes to generate sub-genomic RNA
408 molecules no longer suitable for further replication, making a controlled balance
409 between cleaved and intact genomes crucial to preserve enough replication templates.

410 In this regard, most ribozymes identified here are far from optimal motifs (ie. type I
411 hhrbz seem to lack crucial tertiary interactions[28]), resulting in medium to low self-
412 cleaving activity *in vitro*. Such deviation may allow a significant fraction of viral RNA to
413 evade cleavage and remain competent for replication. Meanwhile, sub-genomic RNA
414 fragments resulting from self-cleavage would serve as templates for translation
415 initiation through an unclear cap-independent mechanism. Although further research
416 will be needed to understand this mechanism, our findings shift the traditional
417 paradigm of small ribozymes as mere processing elements for rolling circle replication
418 of circRNA agents, expanding the evolutionary toolkit of RNA viruses and their
419 biotechnological potential.

420

421 # Methods

422 ## Bioinformatic analysis of viral sequences

423 Computational searches were performed with the INFERNAL 1.1 software[62] using
424 covariance models representing known small-ribozyme classes, and their topological
425 variants, that were obtained from the RFAM 14 database[63]. In addition, newly
426 developed covariance models were included to account for recently identified
427 ribozyme architectures recently described[30,31]. A first screening of a collection of 852
428 thousand contigs (with lengths ranging between 2,000 and 50,000 bp) of DNA or RNA
429 viral origin retrieved from the Genbank NR database (2024) resulted in hundreds of
430 ribozyme hits that were manually inspected. Ribozyme hits present in viral vectors,
431 patented sequences, DNA bacteriophages[16] or in RNA ambiviruses and mitoviruses[31]
432 already described in circRNA replication were discarded, whereas those hits with low
433 E-values such as type I hammerhead (E-val < 10^{-3}), deltavirus (E-val < 0.1) or twister
434 (E-val < 10^{-3}) ribozymes detected in RNA viruses from diverse families were used to
435 build new covariance models to carry out re-screenings
436 (https://github.com/delapenya/RNA_virus_rbz). Analyses of specific RNA viral

437 families showing the presence of small ribozymes and refinement of covariance models
438 were performed iteratively.

439 The consensus features of the ribozyme motifs were calculated based on the ribozyme
440 sequences obtained for each family. Nucleotide frequencies and covariation, as well as
441 the corresponding drawing, were the output of the R2R software[64]. Multiple sequence
442 alignments were performed using MUSCLE[65].

443

444 ## Cloning of ribozyme sequences and transcriptions

445 The sequences corresponding to the hhrbz motifs of the RNA 1 segments of Verticillium
446 dahliae chrysovirus 1 (VdCV1), Penicilium chrysogenum virus and Brassica campestris
447 chrysovirus 1 (Fig. 3) preceded by the T7 RNA polymerase promoter were purchased
448 as gBlock Gene Fragments (Integrated DNA Technologies). The DNA fragments were
449 cloned into a linearized pUC18 vector by BamHI and EcoRI cohesive-end ligation. RNAs
450 of the cloned sequences were synthesized by *in vitro* run-off transcription of the
451 linearized plasmids containing the hhrbzs. The transcription reactions contained
452 40 mM Tris–HCl, pH 8, 6 mM $MgCl_2$, 2 mM spermidine, 0.5 mg/ml RNase-free bovine
453 serum albumin, 0.1% Triton X-100, 10 mM dithiothreitol, 1 mM each of ATP, CTP, GTP,
454 and UTP, 2 U/µl of Ribonuclease Inhibitor (Takara Inc), 20 ng/µl of plasmid DNA, and
455 4 U/µl of T7 RNA polymerase. After incubation at 37°C during the indicated time, the
456 products were fractionated by 10% polyacrylamide gel electrophoresis (PAGE) in the
457 presence of 8 M urea.

458

459 ## Kinetics of self-cleavage

460 Analyses of hhrbz self-cleaving activity under co-transcriptional and post-
461 transcriptional conditions were performed as previously described[66]. Appropriate
462 aliquots of the transcription reactions (progressive smaller volumes were taken at
463 longer incubation times in co-transcriptional assays) were removed at different time
464 intervals, quenched with a fivefold excess of stop solution (8 M urea, 50% formamide,

465 50 mM EDTA, 0.1% xylene cyanol and bromophenol blue) at 0°C, and analyzed as
466 previously described[22,52]. For co-transcriptional cleavage analysis, the uncleaved and
467 cleaved transcripts obtained at different times were separated by PAGE in 10%
468 denaturing gels and detected by Sybr Gold staining (Thermo Fisher Scientific). For
469 post-transcriptional cleavage analysis, uncleaved primary transcripts were eluted by
470 crushing the gel pieces and extracting them with phenol saturated with buffer (Tris–
471 HCl 10 mM, pH 7.5, ethylenediaminetetraacetic acid [EDTA] 1 mM, sodium dodecyl
472 sulfate 0.1%), recovered by ethanol precipitation, and resuspended in deionized sterile
473 water. To determine the cleaving rate constants, uncleaved primary transcripts (from
474 1 nM to 1 μM) were incubated in 20 μl of 50 mM Tris–HCl at the appropriate pH (either
475 7,5 or 8,5) for 1 min at 95 °C and slowly cooled to 25 °C for 15 min. After taking a zero-
476 time aliquot, self-cleavage reactions were triggered by adding $MgCl_2$ at a final
477 concentration of either 1 or 10 mM. Aliquots were removed at the appropriate time
478 intervals and quenched with a fivefold excess of stop solution at 0 °C. The substrate
479 and self-cleaved products were separated by PAGE in 10% denaturing gels and
480 detected by Sybr Gold staining (Thermo Fisher Scientific). In both cases, the product
481 fraction at different times, Ft, was determined by quantitative scanning of the
482 corresponding gel bands and fitted to the equation $F_t=F_\infty(1 - e^{-kt})$, where F_∞ is the
483 product fraction at the reaction endpoint, t is the time in minutes, and k is the first-
484 order rate constant of cleavage (k_{obs}).

485

486 **RACE and northern blot analyses**

487 Analysis of fusarivirus-infected fungi was carried out using the isolate MUT4379 from
488 the Mycotheca Universitatis Taurinensis. Gnomognopsis castanea chrysovirus 1
489 infected isolate 1 was recently described[44]. A symptomless plant of cabbage "Torzella"
490 (*Brassica oleracea* L. var. acephala) infected with BcCV1 (isolate TC-3) was used for
491 plant chysovirus 5' Rapid amplification of cDNA ends (5' RACE) analysis[67].

492 Plant and fungal total RNA was extracted from leaves of cabbage "Torzella" plants and
493 4-day old mycelial liquid cultures grown in PDB following protocols previously

494 described[44,67]. Hirtzman's protocol for 5' RACE was performed as previously described
495 in detail[68]. For each RACE two different primers were designed downstream the
496 predicted ribozyme cleavage site. Regarding GcCV1, the primers used to demonstrate
497 the *in vivo* activity of the ribozymes found in the 5' end of each genomic segment are
498 reported in a previous work[44]. For the RACE demonstrating the *in vivo* activity of the
499 ribozyme found in the intergenic region of the RNA3 of GcCV1, two RACE primers were
500 designed (Supplementary Table 2); the oligonucleotides used to prime RACE for PtFV1
501 and BcCV1 are also displayed in Supplementary Table 2. Briefly, RACE analysis was
502 performed on the 5′ ends of each viral sequence to confirm the presence of a self-
503 cleavage site. The RACE method used[68,69] rely on the synthesis of a cDNA using the
504 specific primers mentioned before and the Superscript IV (Thermo Fisher Scientific,
505 Waltham, MA, USA) reverse transcriptase. Resulting cDNAs were tagged with polyG or
506 polyA using deoxynucleotidyl transferase (Promega, Madison, WI, USA). PCRs were
507 then performed using primer complementary to the polyG or polyA added, and a
508 second specific primer on the viral sequence (Supplementary Table 2). Obtained PCR
509 bands were purified from electrophoresis gel using Zymo gel DNA recovery kit (Zymo
510 Research, Irvine, CA, USA), inserted in a plasmid using the pGEMT easy vector kit
511 (Promega, Madison, WI, USA). Transformed colonies were selected and obtained
512 plasmids were purified using ZR Plasmid Miniprep kit (Zymo Research, Irvine, CA,
513 USA) and sent for Sanger sequencing. For each RACE a minimum of 5 clones were
514 sequenced.

515 Northern blot of fungal extracts for MUT4379 was performed as previously described[70]
516 using a riboprobe (detecting the positive sense viral RNA) obtained by *in vitro*
517 transcription of a cDNA fragment cloned into pGEM-T-Easy (PROMEGA, Madison, WI)
518 corresponding to the genomic region between nt 4,800 and nt 4,980 of the deposited
519 fusarivirus sequence (NCBI NC_028470).

520

521 ## Dual-luciferase (DL) reporter assays

522 The DL assay using fungal mycelia was performed as previously described[46]. Briefly,
523 the pCH-DLst3 vector and PCR-amplified fragments of 5'-UTR and adjacent 72 nt of
524 coding sequence (5'-UTR+) from HvV145S dsRNA2 were digested with *BstE* II and *Not*
525 I, and ligated. The clone obtained was used for transformation of *Cryphonectria*
526 *parasitica* EP155, and mycelia of transformants were subjected to the DL assay as
527 described[46]. The vector pCH-DLst3 carries a codon-optimized Renilla (ORluc) and a
528 Firefly (OFluc) luciferase genes in a bicistronic manner, under the control of the gpd-1
529 promoter/terminator system. *BstE* II and *Not* I recognition sites in between ORluc and
530 OFluc were used for inserting the 5'-UTR and adjacent 72 nt coding cDNA sequence (5'-
531 UTR+; original and mutant variants), expecting that ORluc and OFluc are translated in
532 cap-dependent and cap-independent manner, respectively. *C. parasitica* EP155 was
533 transformed with the different constructs and mycelia of transformants were
534 subjected to DL assay using a dual-luciferase reporter assay system (Promega). A small
535 patch of mycelia was homogenized in a microtube with 200 µl of Cell-Lysate solution,
536 and 10 µl of solution were mixed with 100 µl of the firefly luciferase substrate solution,
537 then the first luminescence intensity was measured using GloMax 20/20 (Promega)
538 with a detection time of 1 s. This was followed by the addition of 100 µl of the Renilla
539 luciferase substrate solution, and the second luminescence measurement.
540 Translational activities were calculated as a ratio of OFluc RLU (relative luminescent
541 unit)/ ORluc RL.

542 The approach used in fungal mycelia was adapted to *Nicotiana benthamiana* plants as
543 previously described[48]. Briefly, a bicistronic construct was made with the two
544 luciferase genes, Rluc and Fluc[71], separated by three stop codons and a small region of
545 ~150 bp either containing a non-coding spacer (pUC Multiple Cloning Site, or MCS of
546 84 bp) sequence as a negative control, or different small self-cleaving motifs (~85-110
547 bp). The entire construct was placed under the control of the 35S promoter and the
548 Nos terminator[48], and cloned into the binary vector pDGB3-alpha1[NO_PRINTED_FORM]
549 through 25 cycles of restriction and ligation reactions, using the restriction enzyme
550 BsaI and T4 DNA ligase (Promega) .Each final plasmid was transferred into

551 *Agrobacterium tumefaciens* strain C58 by electroporation[72]. Overnight-grown bacterial
552 cultures were pelleted and resuspended in agroinfiltration medium, containing 10mM
553 $MgCl_2$, 10mM MES and 150µM acetosyringone, to an optical density at 600 nm of 0.1 to
554 0.2. For transient expression experiments, five-week-old *N. benthamiana* plants were
555 inoculated and maintained under controlled conditions for 6 days. Extracts from 1 cm^2
556 of agroinfiltrated leaf tissue were prepared 5- and 6-days post-infiltration, using 400
557 µl of 0.1M Tris-HCl buffer (pH 7.8). Subsequently, 50 µl of extract were mixed with 45
558 µl of extraction buffer and 5 µl of 10mM luciferase substrate solution (coelenterazine
559 or D-Luciferin to measure Rluc or Fluc activity, respectively). Stock solutions of the
560 substrates were prepared and aliquoted following the manufacturer's protocol
561 (Goldbio). Luminescence from both luciferases in the same extract was measured
562 separately in different wells, using a 2-second integration time. The translational
563 activity was then calculated as the ratio of Fluc RLU/Rluc RLU as in the mycelium assay.
564 Statistical analyses were performed in R (version 4.4.3) using one-way ANOVA to
565 compare experimental groups. Annotated group means in bar plots indicate
566 statistically homogeneous subsets, such that groups sharing the same letter did not
567 differ significantly at $\alpha = 0.05$.

568

569 ## Supplementary Figures and Tables

570 **Supplementary Table 1.** Accession numbers of all the RNA virus genomes/segments
571 containing self-cleaving ribozymes identified in this study.

572 EXCEL FILE

573

574 **Supplementary Table 2.** Oligonucleotide sequences and their specific use in this
575 work.

576

Oligonucleotide Name	Sequence (5' to 3')	Use
BcCV1-RNA1-77Rev	CAAAGATGCGTTTTCCCATGC	RACE
BcCV1-RNA1-87Rev	TGCTTTGCAGCACCGTTTA	RACE
BcCV1-RNA1-88NRev	TCGTCTGTGTAGCAACACTAAC	RACE
BcCV1-RNA2-81Rev	GCGCAAGCAACCAGGTTCA	RACE
BcCV1-RNA2-82Rev	CCTTCCATTGTGCTATTAAGGTAT	RACE
BcCV1-RNA3-85Rev	CTCTTCATGTTGCATGAATTCG	RACE
BcCV1-RNA3-86Rev	TGCAGACGTGTTTTCCATTGT	RACE
Fusari-5000Rev	TGTTTCCTTGACGCTCGTGT	RACE
Fusari-4800For	ACCCGGAGAGCTCAAATGTT	RACE
Fusari-4980Rev	GTAACTTAAGAAGTTTGGCT	RACE
GcCV1_RNA3_1163Rev	AATCTCTCCGCCGCTGTCGT	RACE
GcCV1_RNA3_1104Rev	TGTTCTCCCGTTCCTCGGTG	RACE

577

578

Supplementary Figures

Supplementary Fig. 1. (A) Detailed consensus models and secondary structures of the hammerhead ribozymes either with long helix II (left, based on 26 ribozyme sequences) or short helix II (right, based on 62 ribozyme sequences) from chrysovirus genomes. (B) Consensus model of the hammerhead ribozyme present in most fusarivirus genomes (based on 123 ribozyme sequences). The legend inset applies to the three models shown. (C) Three representative examples of hammerhead ribozymes from fusarivirus genomes with variable stem lengths for helix I, II and III. The site of ribozyme-mediated RNA cleavage is identified by an arrowhead. Consensus models were built as previously described[64].

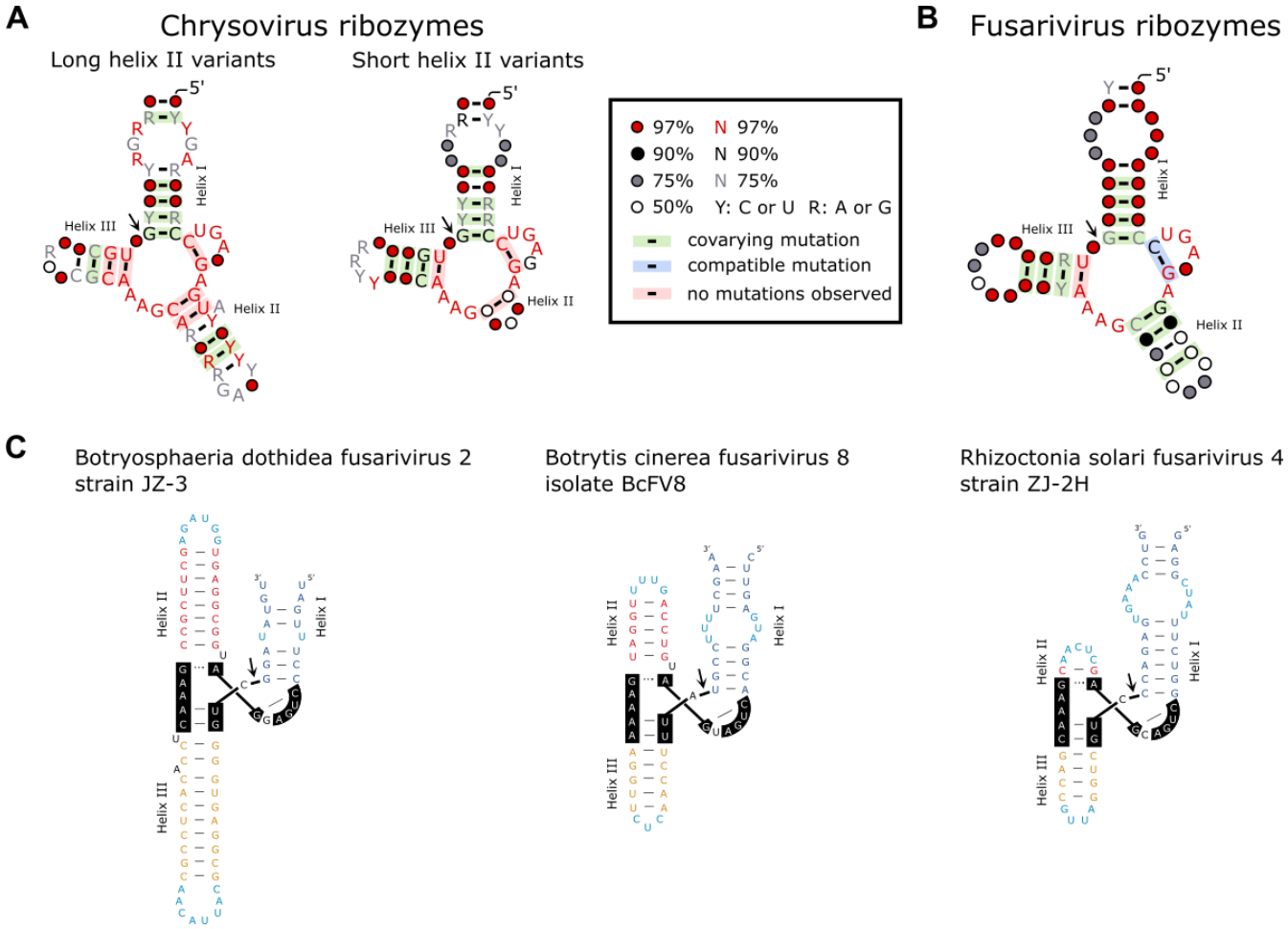

Supplementary Fig. 2. Representative assays of self-cleavage kinetics for four hammerhead ribozymes encoded in fungal and plant RNA viruses. (A) Structure of the hammerhead ribozyme from Verticillium dahliae chrysovirus 1, RNA 1 (left), a 10% PAGE showing the resulting RNAs after different transcription times (standard conditions, pH 7.5, 1 mM Mg^{2+}) (center), and the kinetic analysis and quantification graph of the cleavage rates under these co-transcriptional conditions (right). (B) Structure of the hammerhead ribozyme from Brassica campestris chrysovirus (left), two 10% PAGEs showing post-transcriptional assays of self-cleavage with purified RNA of this ribozyme incubated at pH 8.5 and 1 or 10 mM Mg^{2+}(Methods) (right), and their kinetic analysis and quantification graph of the cleavage rates (bottom). (C) Structure of the hammerhead ribozyme from Penicillium chrysogenum virus, RNA 1 (left), a 10% PAGE showing a post-transcriptional assay of self-cleavage with purified RNA of this ribozyme incubated at pH 8.5 and 1 or 10 mM Mg^{2+}(Methods) (right), and their kinetic analysis and quantification graph of the observed cleavage rates (bottom). (D) Structure of the hammerhead ribozyme from the Rosellinia necatrix megabirnavirus 1 (RnMBV1) (left), a 10% PAGE showing a co-transcriptional self-cleavage assay (center) and quantification graph of the cleavage rate.

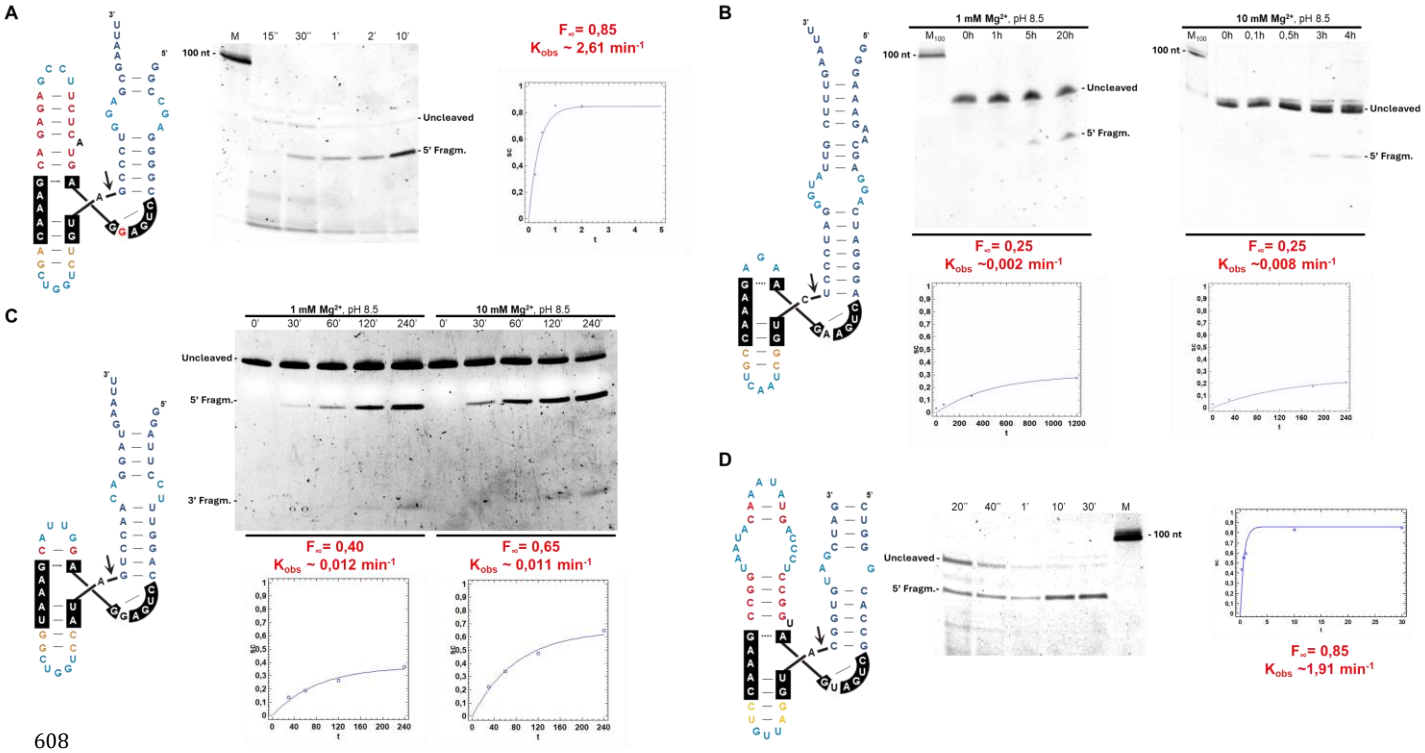

Supplementary Fig. 3. (A) Representative examples of hammerhead ribozymes (hhrbzs) detected in the UTRs of two ssRNA fusariviruses. (B) An example of a dsRNA megabirnavirus-like genome showing the presence of a hhrbz in its 5'-UTR and a deltavirus ribozyme encoded within the predicted RNA dependent RNA polymerase (RdRp) ORF. Sites of ribozyme self-cleavage are indicated by arrows.

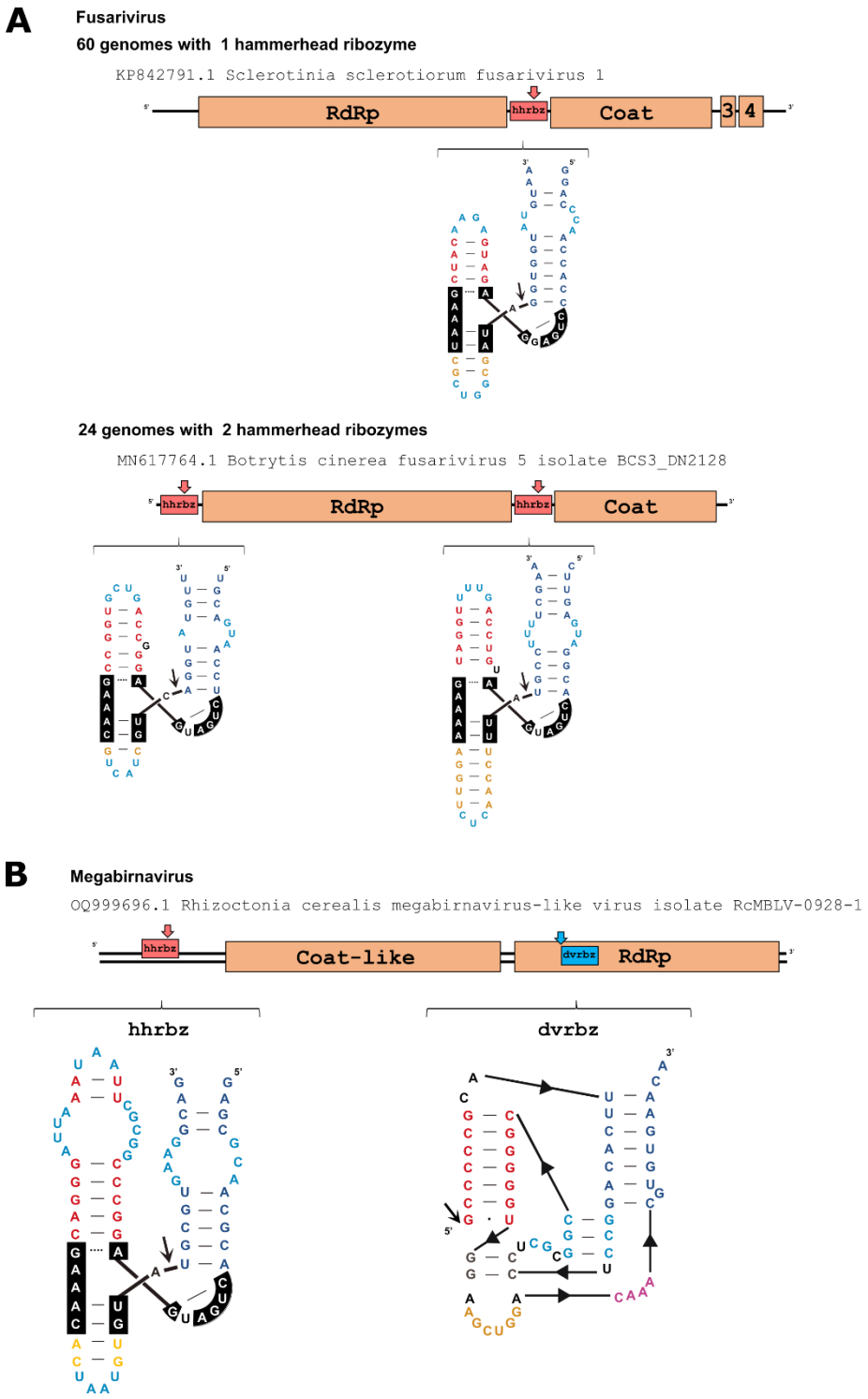

Supplementary Fig. 4. Predicted subgenomic circRNAs detected in (A) Sclerotium rolfsii, (B) Telephora terrestris, (C) Letinula edodes and (D) Phlebiopsis gigantea toti-like mycoviruses containing close ribozyme pairs. Resulting RNAs after double self-cleavage show quasi-rod like structures (circular Jupiter plots are shown at the right), sizes multiple of 3 nt, and absence of stop codons (potentially encoding endless ORFs with protein sequences shown at the insets) as similarly described for zetaviruses[31,32] (in panel (D), two previously reported Zetavirus genomes are shown for comparison). Hyp; hypothetical. polyprot; polyprotein. hhrbz; hammerhead ribozyme. dvrbz; deltavirus ribozyme. RdRp; RNA dependent RNA polymerase.

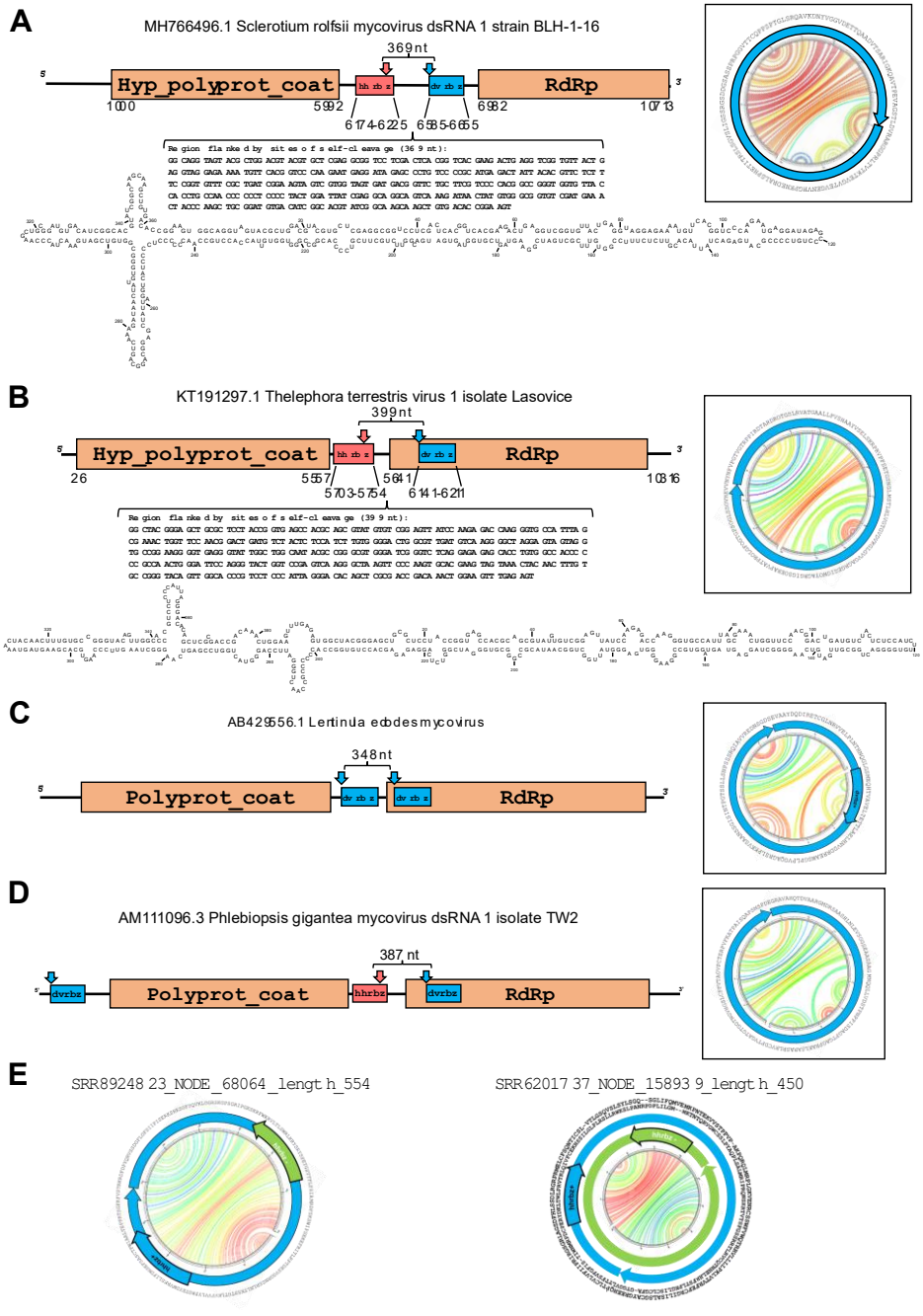

Supplementary Fig. 5. Twister ribozymes (twrbz) motifs detected in the RNA genomes of (A) phelgivirus-like and (B) tombusvirus-like sequences. Highly conserved nucleotides and unexpected changes in the consensus structure of most twrbz motifs are depicted in red and blue, respectively.

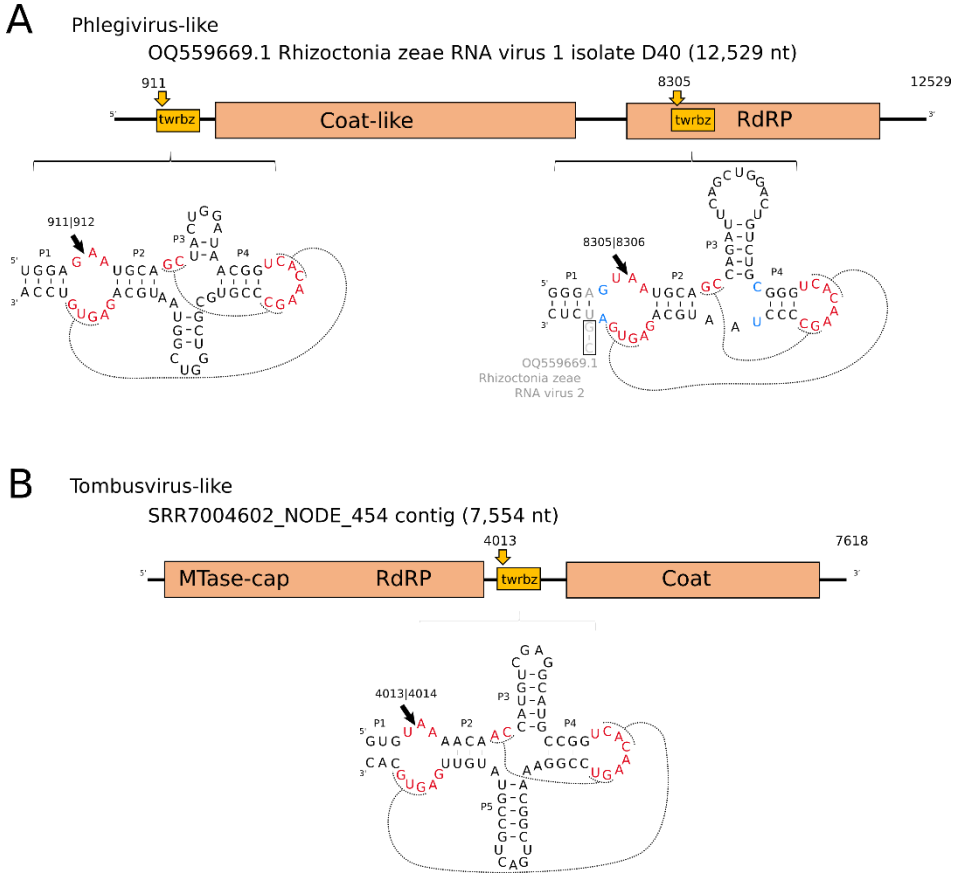

Supplementary Fig. 6. 5' RACE of Brassica campestris chrysovirus 1 (BcCV-1) from infected cabbage Torzella plants. (A) Schematic representation of the BcCV-1 hhrbzs in the 5'-UTRs of each of the three genomic RNA segments. (B) Schematic representation of the aproximated locations of the oligos used for the RACE experiments and the expected sizes of the PCR products resulting from the full-length and self-cleaved RNAs (C) Agarose gel analysis of 5' RACE PCR of BcCV-1 RNA1, RNA2 and RNA3 (lanes 1, 2 and 3, respectively) shows two bands corresponding to the amplification of the full-length (upper and more abundant band) and the self-cleaved (lower band) RNAs. For the RNA1 (lane 1), a nested PCR, using a reverse BcCV-1 RNA1 (BcCV1-RNA1-88NRev, Supplementary Table S2), nested to the primer used in the first RACE amplification (BcCV1-RNA1-87Rev, Supplementary Table S2), is shown. M, DNA molecular weight marker (100 bp DNA ladder, Thermo Fisher). (C) Sequencing electropherograms of the cloned RACE product of smaller size for each RNA genomic segment. The 5' end coincides with that predicted to be generated by the hhrbz self-cleavage (indicated by arrows).

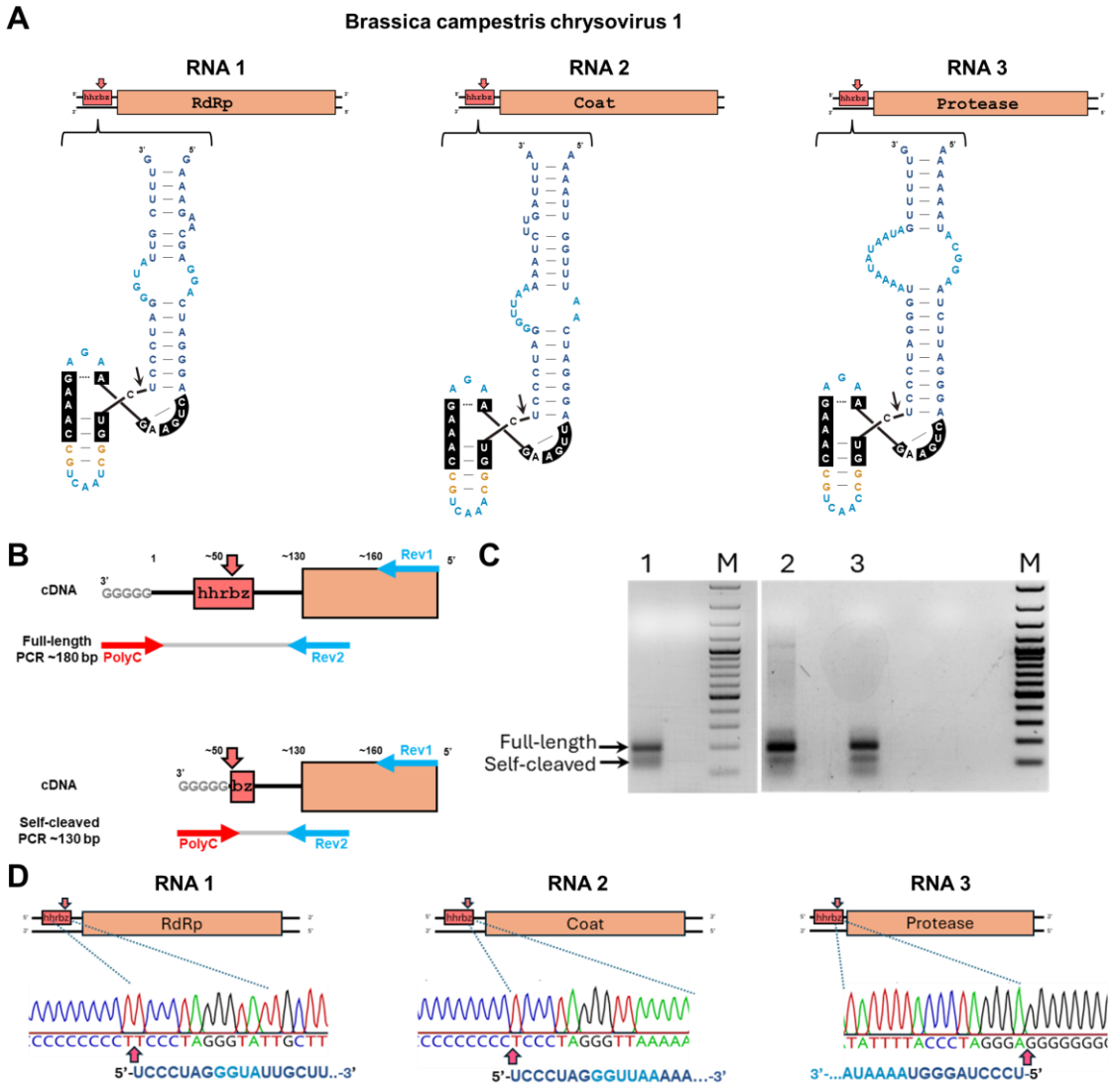

Supplementary Fig. 7. 5' RACE of Gnomoniopsis castaneae chrysovirus 1 (GcCV-1) from infected *G. castaneae* isolate 1[44]. Schematic representation of GcCV-1 RNAs, hammerhead ribozymes (hhrbz) secondary structure and sequencing electropherograms of the cloned RACE product of smaller size for each (A) RNA 1, (B) RNA 2 (C) RNA 3 and (D) RNA 4 genomic segments. Hhrbzs are present in all the 5'-UTR of RNAs, whereas RNA3 shows a second intergenic hhrbz motif between the two conserved ORFs (3a and 3b). The 5' ends of the sequencing electropherograms coincide with those predicted to be generated by the hhrbz self-cleavage (indicated by arrows). (E) Agarose gel analysis of 5' RACE PCR (lane 1) and 3'RACE PCR (lane 2) of GcCV-1 RNA2. Lane 1 shows two bands corresponding to the amplification of the full-length (upper band) and the self-cleaved (lower band) RNAs. M; DNA molecular weight marker of 100 bp DNA (Thermo Fisher). RdRp; RNA dependent RNA polymerase. CP; coat protein. ORF; open reading frame.

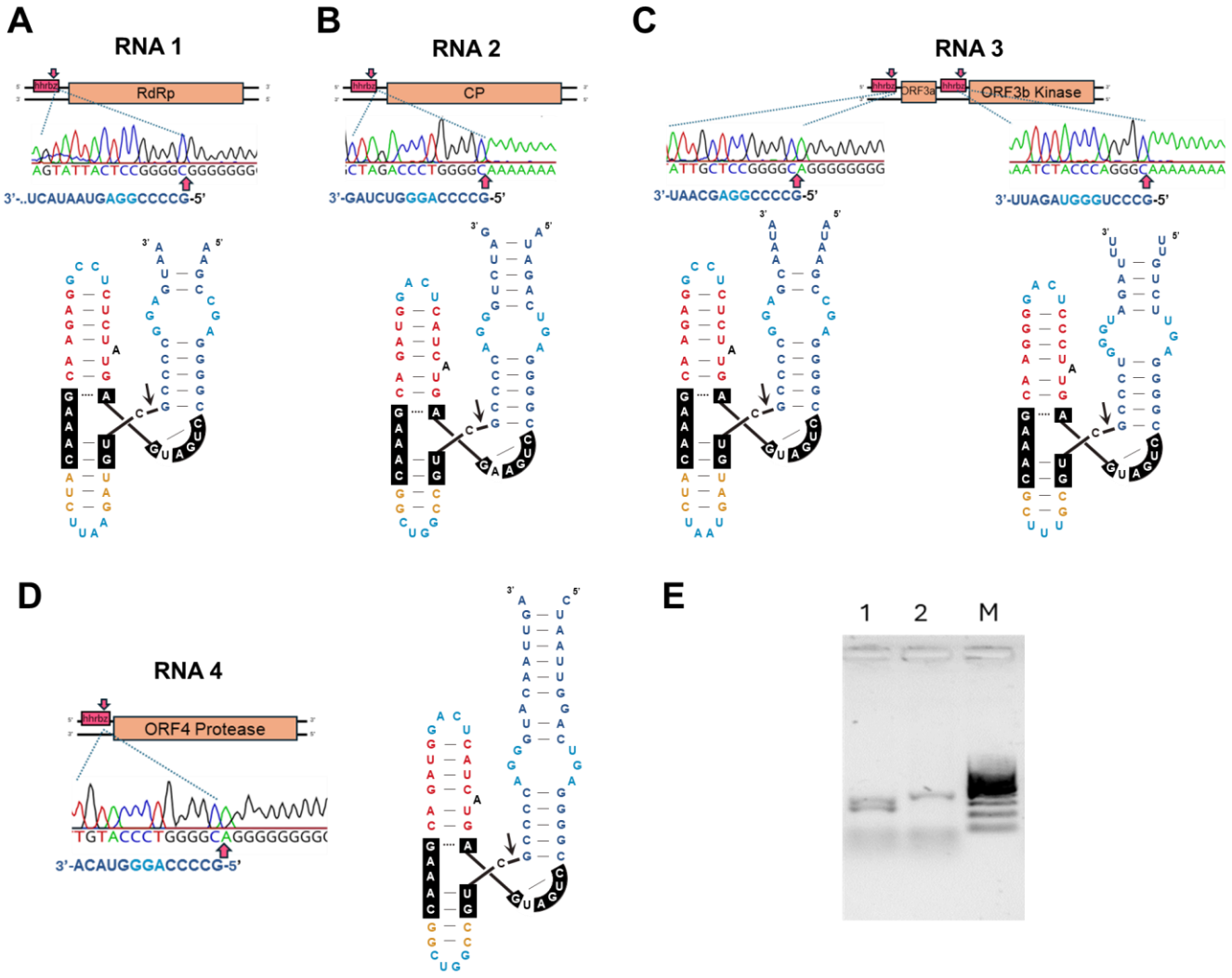

Supplementary Fig. 8. 5' RACE of Pleospora typhicola fusarivirus 1 (PtFV1) from infected MUT 4379 [45]. (A) Genome organization, with the position of the hammerhead ribozyme (hhrbz) placed in the intergenic region. The secondary structure of the ribozyme is also displayed (right), as well as the sequence electropherogram showing the 5' end of the cleavage site (red arrow). (B) Northern blot analysis of RNA extracts from virus-infected isolate MUT4379 and virus-free *Rhizoctonia solani* isolate IEE-16[73]. On the left panel, red arrows indicate the PtFV1 genomic RNA (gRNA) and PtFV1 sgRNA positions, while green arrows indicate some possible cross-hybridization with the two fungal ribosomal RNAs. The right panel shows a methylene blue stain of the membrane displaying the two ribosomal RNA bands.

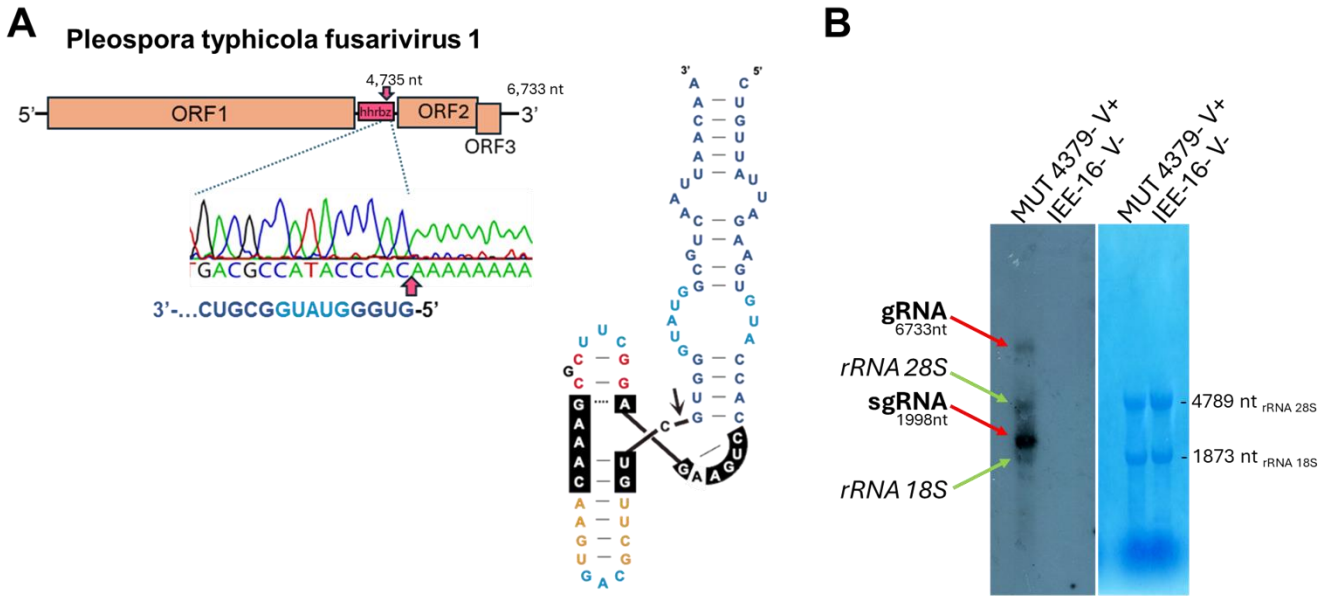

Supplementary Fig. 9. (A) Top: schematic representation of a type I hammerhead ribozyme (hhrbz) from Schistosoma mansoni with tertiary loop-loop interactions indicated by dotted lines. Bottom: 3D-structure (pdb 3ZD5) showing the central conserved core in black and the three stems I, II, and III in blue, red, and yellow, respectively; loops are not shown. Similarly, schematic (top) and 3D structures (bottom) of (B) the Hv145S-RNA2 hhrbz (predicted through the Alphafold 3 server[74]), (C) Hepatitis A virus (HAV) IRES domain V (pdb 6mwn)[61] and (D) the J-K domain of the encephalomyocarditis virus (EMCV) IRES element (pdb 2nbx)[59].

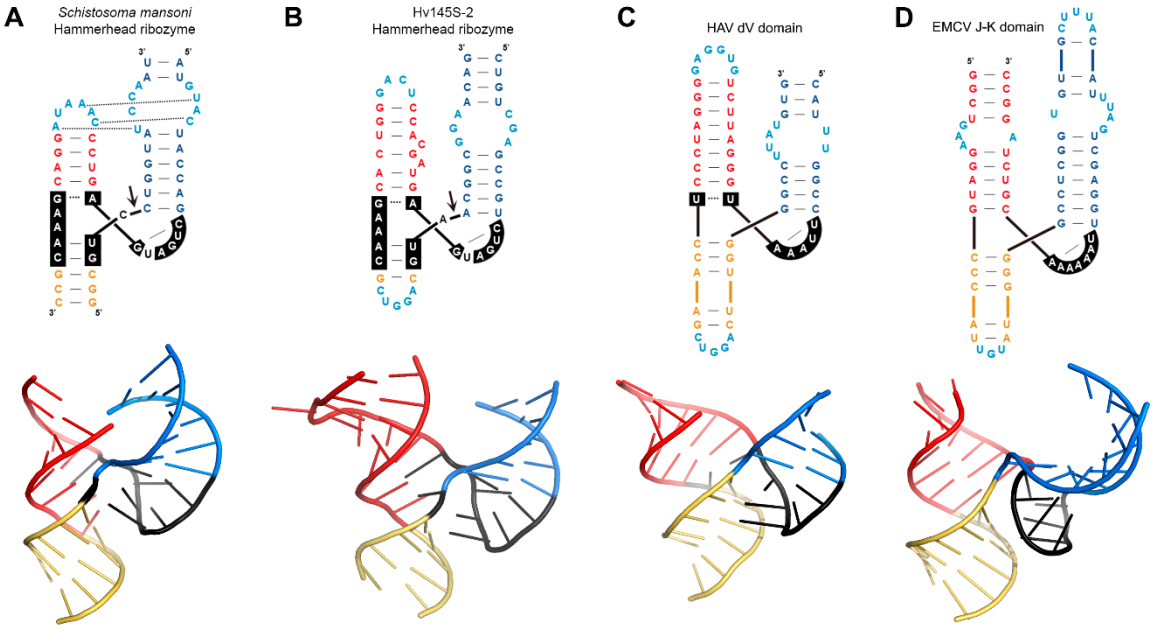

Supplementary Fig. 10. Three dimensional models for (A) the hammerhead ribozyme from *Schistosoma mansoni* retrozymes (pdb 3ZD5, central core and stems, but not interacting loops 1 and 2, are shown), (B) the human Hepatitis Delta ribozyme (pdb 1DRZ), (C) the Hepatitis A virus IRES dV core domain (pdb 6mwn) and (D) the encephalomyocarditis virus IRES J-K core domain (pdb 2nbx).

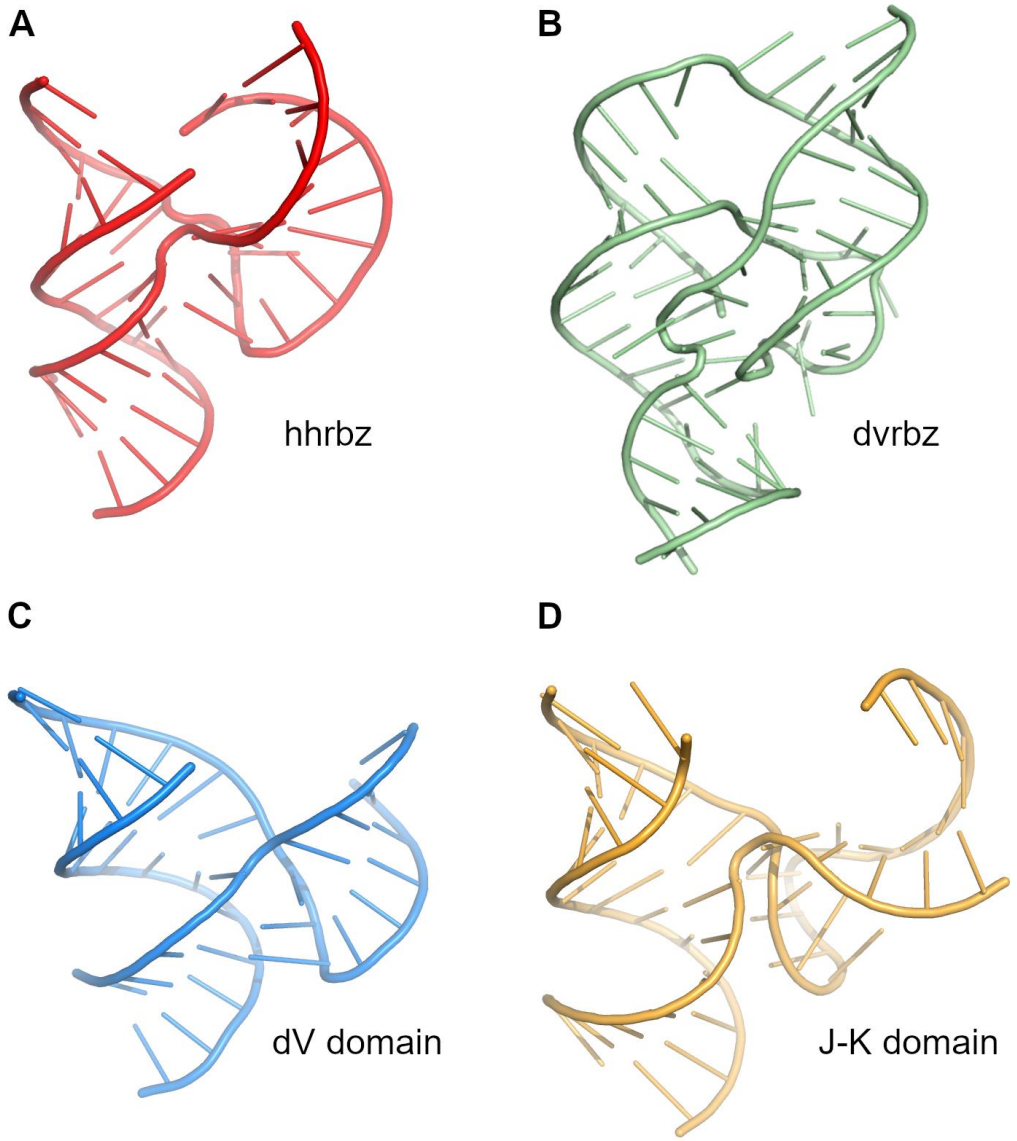

Acknowledgments

This work was funded by: University of Valencia Margarita Salas Fellowship MS21-067 (MJLG); Generalitat Valenciana Grant PROMETEO CIPROM/2022/21 (MdlP); Ministerio de Ciencia, Innovacion y Universidades de España-FEDER grant PID2024-162245NB-I00 (MdlP). We are grateful to Daniela Alio and Maria Minutolo for providing plants infected by Brassica campestris chrysovirus 1.

References

1. Woese, C. R. The fundamental nature of the genetic code: prebiotic interactions between polynucleotides and polyamino acids or their derivatives. *Proc Natl Acad Sci U S A* **59**, 110–117 (1968).

2. Crick, F. H. The origin of the genetic code. *J Mol Biol* **38**, 367–379 (1968).

3. Gilbert, W. The RNA World. *Nature* **319**, 618 (1986).

4. Flores, R., Gago-Zachert, S., Serra, P., Sanjuan, R. & Elena, S. F. Viroids: survivors from the RNA world? *Annu Rev Microbiol* **68**, 395–414 (2014).

5. Forterre, P. The origin of viruses and their possible roles in major evolutionary transitions. *Virus Res.* **117**, 5–16 (2006).

6. Prody, G. A., Bakos, J. T., Buzayan, J. M., Schneider, I. R. & Bruening, G. Autolytic processing of dimeric plant virus satellite RNA. *Science (1979).* **231**, 1577–1580 (1986).

7. Hutchins, C. J., Rathjen, P. D., Forster, A. C. & Symons, R. H. Self-cleavage of plus and minus RNA transcripts of avocado sunblotch viroid. *Nucleic Acids Res.* **14**, 3627–3640 (1986).

8. Buzayan, J. M., Gerlach, W. L. & Bruening, G. Satellite tobacco ringspot virus RNA: A subset of the RNA sequence is sufficient for autolytic processing. *Proc Natl Acad Sci U S A* **83**, 8859–8862 (1986).

9. Kuo, M. Y., Sharmeen, L., Dinter-Gottlieb, G. & Taylor, J. Characterization of self-cleaving RNA sequences on the genome and antigenome of human hepatitis delta virus. *J Virol* **62**, 4439–4444 (1988).

10. Saville, B. J. & Collins, R. A. A site-specific self-cleavage reaction performed by a novel RNA in Neurospora mitochondria. *Cell* **61**, 685–696 (1990).

722 11. Winkler, W. C., Nahvi, A., Roth, A., Collins, J. A. & Breaker, R. R. Control of gene
723 expression by a natural metabolite-responsive ribozyme. *Nature* **428**, 281–286
724 (2004).

725 12. Roth, A. *et al.* A widespread self-cleaving ribozyme class is revealed by
726 bioinformatics. *Nat Chem Biol* **10**, 56–60 (2014).

727 13. Weinberg, Z. *et al.* New classes of self-cleaving ribozymes revealed by
728 comparative genomics analysis. *Nat. Chem. Biol.* **11**, 606–610 (2015).

729 14. Ferbeyre, G., Smith, J. M. & Cedergren, R. Schistosome satellite DNA encodes
730 active hammerhead ribozymes. *Mol Cell Biol* **18**, 3880–3888 (1998).

731 15. Epstein, L. M. & Gall, J. G. Self-cleaving transcripts of satellite DNA from the
732 newt. *Cell* **48**, 535–543 (1987).

733 16. Hammann, C., Luptak, A., Perreault, J. & de la Peña, M. The ubiquitous
734 hammerhead ribozyme. *RNA* **18**, 871–885 (2012).

735 17. De la Peña, M. & García-Robles, I. Ubiquitous presence of the hammerhead
736 ribozyme motif along the tree of life. *RNA* **16**, 1943–1950 (2010).

737 18. Webb, C. H. T., Riccitelli, N. J., Ruminski, D. J. & Lupták, A. Widespread
738 occurrence of self-cleaving ribozymes. *Science (1979).* **326**, 953 (2009).

739 19. De la Peña, M. & Garcia-Robles, I. Intronic hammerhead ribozymes are
740 ultraconserved in the human genome. *EMBO Rep* **11**, 711–716 (2010).

741 20. Salehi-Ashtiani, K., Luptak, A., Litovchick, A. & Szostak, J. W. A genomewide
742 search for ribozymes reveals an HDV-like sequence in the human CPEB3 gene.
743 *Science (1979).* **313**, 1788–1792 (2006).

744 21. Ruminski, D. J., Webb, C. H. T., Riccitelli, N. J., Lupta, A. & Luptak, A. Processing
745 and translation initiation of non-long terminal repeat retrotransposons by
746 hepatitis delta virus (HDV)-like self-cleaving ribozymes. *J Biol Chem* **286**,
747 41286–41295 (2011).

748 22. Cervera, A. & de la Peña, M. Eukaryotic penelope-like retroelements encode
749 hammerhead ribozyme motifs. *Mol Biol Evol* **31**, 2941–2947 (2014).

750 23. Eickbush, D. G. & Eickbush, T. H. R2 retrotransposons encode a self-cleaving
751 ribozyme for processing from an rRNA cotranscript. *Mol Cell Biol* **30**, 3142–
752 3150 (2010).

753 24. Cervera, A., Urbina, D. & de la Peña, M. Retrozymes are a unique family of non-
754 autonomous retrotransposons with hammerhead ribozymes that propagate in
755 plants through circular RNAs. *Genome Biol* **17**, 135 (2016).

25. Cervera, A. & de la Peña, M. Small circRNAs with self-cleaving ribozymes are highly expressed in diverse metazoan transcriptomes. *Nucleic Acids Res.* **48**, 5054–5064 (2020).

26. Liu, G. *et al.* The function of twister ribozyme variants in non-LTR retrotransposition in Schistosoma mansoni. *Nucleic Acids Res.* **49**, 10573–10588 (2021).

27. Salehi-Ashtiani, K. & Szostak, J. W. In vitro evolution suggests multiple origins for the hammerhead ribozyme. *Nature* **414**, 82–84 (2001).

28. De la Peña, M., Gago, S. & Flores, R. Peripheral regions of natural hammerhead ribozymes greatly increase their self-cleavage activity. *EMBO J* **22**, 5561–5570 (2003).

29. Martick, M. & Scott, W. G. Tertiary contacts distant from the active site prime a ribozyme for catalysis. *Cell* **126**, 309–320 (2006).

30. Eckert, I., Friedrich, R., Weinberg, C. E. & Weinberg, Z. Discovery of natural non-circular permutations in non-coding RNAs. *Nucleic Acids Res.* **51**, 2850–2861 (2023).

31. Forgia, M. *et al.* Hybrids of RNA viruses and viroid-like elements replicate in fungi. *Nature Communications 2023 14:1* **14**, 1–11 (2023).

32. Edgar, R. C. *et al.* Petabase-scale sequence alignment catalyses viral discovery. *Nature 2022* **602**, 1–6 (2022).

33. Weinberg, C. E., Olzog, V. J., Eckert, I. & Weinberg, Z. Identification of over 200-fold more hairpin ribozymes than previously known in diverse circular RNAs. *Nucleic Acids Res.* **49**, 6375–6388 (2021).

34. Lee, B. D. *et al.* Mining metatranscriptomes reveals a vast world of viroid-like circular RNAs. *Cell* **186**, 646-661.e4 (2023).

35. Zheludev, I. N. *et al.* Viroid-like colonists of human microbiomes. *bioRxiv* 2024.01.20.576352 (2024) doi:10.1101/2024.01.20.576352.

36. Arkhipova, I. R., Yushenova, I. A. & Rodriguez, F. Giant Reverse Transcriptase-Encoding Transposable Elements at Telomeres. *Mol. Biol. Evol.* **34**, 2245–2257 (2017).

37. Epstein, L. M. & Pabon-Pena, L. M. Alternative modes of self-cleavage by newt satellite 2 transcripts. *Nucleic Acids Res* **19**, 1699–1705 (1991).

38. Cao, Y. fen *et al.* Genomic characterization of a novel dsRNA virus detected in the phytopathogenic fungus Verticillium dahliae Kleb. *Virus Res.* **159**, 73–78 (2011).

791 39. Zhang, R. *et al.* A novel single-stranded RNA virus isolated from a
792 phytopathogenic filamentous fungus, Rosellinia necatrix, with similarity to
793 hypo-like viruses. *Front. Microbiol.* **5**, 92402 (2014).

794 40. Chiba, S. *et al.* ICTV Virus Taxonomy Profile: Fusariviridae 2024: This article is
795 part of the ICTV Virus Taxonomy Profiles collection. *Journal of General Virology*
796 **105**, 001973 (2024).

797 41. Chiba, S. *et al.* A novel bipartite double-stranded RNA mycovirus from the white
798 root rot fungus Rosellinia necatrix: Molecular and biological characterization,
799 taxonomic considerations, and potential for biological control. *J. Virol.* **83**,
800 12801–12812 (2009).

801 42. Li, S. *et al.* Sixteen Novel Mycoviruses Containing Positive Single-Stranded RNA,
802 Double-Stranded RNA, and Negative Single-Stranded RNA Genomes Co-Infect a
803 Single Strain of Rhizoctonia zeae. *Journal of Fungi* **10**, 30 (2024).

804 43. Zhang, J. *et al.* The genome sequence of Brassica campestris chrysovirus 1, a
805 novel putative plant-infecting tripartite chrysovirus. *Arch. Virol.* **162**, 1107–
806 1111 (2017).

807 44. Ferilli, F., Lione, G., Gonthier, P., Turina, M. & Forgia, M. First detection of
808 mycoviruses in Gnomoniopsis castaneae suggests a putative horizontal gene
809 transfer event between negative-sense and double-strand RNA viruses.
810 *Virology* 110057 (2024) doi:10.1016/J.VIROL.2024.110057.

811 45. Nerva, L. *et al.* Multiple approaches for the detection and characterization of
812 viral and plasmid symbionts from a collection of marine fungi. *Virus Res.* **219**,
813 22–38 (2016).

814 46. Chiba, S., Jamal, A. & Suzuki, N. First evidence for internal ribosomal entry sites
815 in diverse fungal virus genomes. *mBio* **9**, (2018).

816 47. Doudna, J. A. Hammerhead ribozyme structure: U-turn for RNA structural
817 biology. *Structure* **3**, 747–750 (1995).

818 48. Sarrion-Perdigones, A. *et al.* GoldenBraid 2.0: A Comprehensive DNA Assembly
819 Framework for Plant Synthetic Biology. *Plant Physiol.* **162**, 1618–1631 (2013).

820 49. Kristoffersen, E. L., Burman, M., Noy, A. & Holliger, P. Rolling Circle RNA
821 Synthesis Catalysed by RNA. *Elife* **11**, (2022).

822 50. Jimenez, R. M., Polanco, J. A. & Luptak, A. Chemistry and Biology of Self-Cleaving
823 Ribozymes. *Trends Biochem Sci* **40**, 648–661 (2015).

824 51. De la Peña, M., Garcia-Robles, I. & Cervera, A. The Hammerhead Ribozyme: A
825 Long History for a Short RNA. *Molecules* **22**, 1–11 (2017).

826 52. De La Peña, M., Ceprian, R., Casey, J. L. & Cervera, A. Hepatitis delta virus-like
827 circular RNAs from diverse metazoans encode conserved hammerhead
828 ribozymes. *Virus Evol.* **7**, (2021).

829 53. Perreault, J. *et al.* Identification of hammerhead ribozymes in all domains of life
830 reveals novel structural variations. *PLoS Comput Biol* **7**, e1002031 (2011).

831 54. Khvorova, A., Lescoute, A., Westhof, E. & Jayasena, S. D. Sequence elements
832 outside the hammerhead ribozyme catalytic core enable intracellular activity.
833 *Nat Struct Biol* **10**, 708–712 (2003).

834 55. De la Peña, M., Dufour, D. & Gallego, J. Three-way RNA junctions with remote
835 tertiary contacts: a recurrent and highly versatile fold. *RNA* **15**, 1949–1964
836 (2009).

837 56. Schultz, E. P., Vasquez, E. E. & Scott, W. G. Structural and catalytic effects of an
838 invariant purine substitution in the hammerhead ribozyme: Implications for
839 the mechanism of acid-base catalysis. *Acta Crystallogr. D Biol. Crystallogr.* **70**,
840 2256–2263 (2014).

841 57. Martínez-Salas, E., Francisco-Velilla, R., Fernandez-Chamorro, J., Lozano, G. &
842 Diaz-Toledano, R. Picornavirus IRES elements: RNA structure and host protein
843 interactions. *Virus Res.* **206**, 62–73 (2015).

844 58. Kolupaeva, V. G., Pestova, T. V., Hellen, C. U. T. & Shatsky, I. N. Translation
845 Eukaryotic Initiation Factor 4G Recognizes a Specific Structural Element within
846 the Internal Ribosome Entry Site of Encephalomyocarditis Virus RNA. *Journal*
847 *of Biological Chemistry* **273**, 18599–18604 (1998).

848 59. Imai, S., Kumar, P., Hellen, C. U. T., D'Souza, V. M. & Wagner, G. An accurately
849 preorganized IRES RNA structure enables eIF4G capture for initiation of viral
850 translation. *Nature Structural & Molecular Biology 2016 23:9* **23**, 859–864
851 (2016).

852 60. Brown, E. A., Day, S. P., Jansen, R. W. & Lemon, S. M. The 5' nontranslated region
853 of hepatitis A virus RNA: secondary structure and elements required for
854 translation in vitro. *J. Virol.* **65**, 5828–5838 (1991).

855 61. Koirala, D. *et al.* A conserved RNA structural motif for organizing topology
856 within picornaviral internal ribosome entry sites. *Nature Communications 2019*
857 *10:1* **10**, 1–13 (2019).

858 62. Nawrocki, E. P. & Eddy, S. R. Infernal 1.1: 100-fold faster RNA homology
859 searches. *Bioinformatics* **29**, 2933–2935 (2013).

860 63. Kalvari, I. *et al.* Rfam 14: expanded coverage of metagenomic, viral and
861 microRNA families. *Nucleic Acids Res.* **49**, D192–D200 (2021).

862 64. Weinberg, Z. & Breaker, R. R. R2R - software to speed the depiction of aesthetic
863 consensus RNA secondary structures. *BMC Bioinformatics* **12**, 1–9 (2011).

864 65. Edgar, R. C. MUSCLE: multiple sequence alignment with high accuracy and high
865 throughput. *Nucleic Acids Res.* **32**, 1792–1797 (2004).

866 66. Long, D. M. & Uhlenbeck, O. C. Kinetic characterization of intramolecular and
867 intermolecular hammerhead RNAs with stem II deletions. *Proc Natl Acad Sci U*
868 *S A* **91**, 6977–6981 (1994).

869 67. Minutolo, M. *et al.* A polyvalent tool for detecting coguviruses in multiple hosts
870 allowed the identification of a novel seed-transmitted coguvirus infecting
871 Brassicaceae. *Phytopathology* https://doi.org/10.1094/PHYTO-10-23-0362-
872 R/ASSET/IMAGES/LARGE/PHYTO-10-23-0362-RT2.JPEG (2023)
873 doi:10.1094/PHYTO-10-23-0362-R/ASSET/IMAGES/LARGE/PHYTO-10-23-
874 0362-RT2.JPEG.

875 68. Rastgou, M. *et al.* Molecular characterization of the plant virus genus
876 Ourmiavirus and evidence of inter-kingdom reassortment of viral genome
877 segments as its possible route of origin. *J. Gen. Virol.* **90**, 2525 (2009).

878 69. Hirzmann, J., Luo, D., Hahnen, J. & Hobom, G. Determination of messenger RNA
879 5′-ends by reverse transcription of the cap structure. *Nucleic Acids Res.* **21**,
880 3597–3598 (1993).

881 70. Sutela, S. *et al.* The virome from a collection of endomycorrhizal fungi reveals
882 new viral taxa with unprecedented genome organization. *Virus Evol.* **6**, (2020).

883 71. McNabb, D. S., Reed, R. & Marciniak, R. A. Dual Luciferase Assay System for
884 Rapid Assessment of Gene Expression in Saccharomyces cerevisiae. *Eukaryot.*
885 *Cell* **4**, 1539 (2005).

886 72. Wieland, W. H., Lammers, A., Schots, A. & Orzáez, D. V. Plant expression of
887 chicken secretory antibodies derived from combinatorial libraries. *J. Biotechnol.*
888 **122**, 382–391 (2006).

889 73. Picarelli, M. A. S. C. *et al.* Extreme diversity of mycoviruses present in isolates of
890 rhizoctonia solani AG2-2 LP from Zoysia japonica from Brazil. *Front. Cell. Infect.*
891 *Microbiol.* **9**, 457597 (2019).

892 74. Abramson, J. *et al.* Accurate structure prediction of biomolecular interactions
893 with AlphaFold 3. *Nature 2024* 1–3 (2024) doi:10.1038/s41586-024-07487-w.

894